DRI. No. 135
Technical Report: MRI - 290

DOE/JPL - 955676-2
Distribution Category UC - 63

ANALYSIS OF DEFECT STRUCTURE IN SILICON

CHARACTERIZATION OF SAMPLES FROM UCP INGOT 5848-13C

**Silicon Sheet Growth Development
for the Large Area Silicon Sheet Task of
the Low-Cost Solar Array Project.**

INTERIM REPORT

by
R. Natesh
T. Guyer
G. B. Stringfellow

August, 1982

JPL Contract No. 955676

The JPL Low-Cost Silicon Solar Array Project is sponsored by the U.S. Department of Energy and forms part of the Solar Photovoltaic Conversion Program to initiate a major effort toward the development of low-cost solar arrays. This work was performed for the Jet Propulsion Laboratory, California Institute of Technology, by agreement between NASA and DOE.

MRI Materials Research, Inc.

Research
Development
Consulting and Testing
Of Materials

700 South 790 East
Centerville, Utah 84014
Telephone (801) 298-4000

DRL No. 135
Technical Report: MRI - 290

DOE/JPL - 955676-1
Distribution Category UC - 63

ANALYSIS OF DEFECT STRUCTURE IN SILICON

CHARACTERIZATION OF SAMPLES FROM UCP INGOT 5848-13C

**Silicon Sheet Growth Development
for the Large Area Silicon Sheet Task of
the Low-Cost Solar Array Project.**

INTERIM REPORT

by
R. Natesh
T. Guyer
G. B. Stringfellow

August, 1982

JPL Contract No. 955676

The JPL Low-Cost Silicon Solar Array Project is sponsored by the U.S. Department of Energy and forms part of the Solar Photovoltaic Conversion Program to initiate a major effort toward the development of low-cost solar arrays. This work was performed for the Jet Propulsion Laboratory, California Institute of Technology, by agreement between NASA and DOE.

MRI Materials Research, Inc.

Research
Development
Consulting and Testing
Of Materials

700 South 790 East
Centerville, Utah 84014
Telephone (801) 298-4000

TECHNICAL CONTENT STATEMENT

This report was prepared as an account of work sponsored by the United States Government. Neither the United States nor the United States Department of Energy, nor any of their employees, nor any of their contractors, subcontractors, or their employees, make any warranty, express or implied, or assumes any legal liability or responsibility for the accuracy, completeness, or usefulness of any information, apparatus, product, or process disclosed, or represents that its use would not infringe privately-owned rights.

CONTENTS

LIST OF FIGURES

LIST OF TABLES

SECTION I

SUMMARY

Statistically significant quantitative structural imperfection measurements were made on samples from Ubiquitous Crystalline Process (UCP) Ingot 5848 - 13C. Important trends were noticed between the measured data , cell efficiency, and diffusion length. Grain boundary substructure appears to have important effect on conversion efficiency of solar cells from Semix material. Quantitative microscopy measurements gives statistically significant information compared to other micro - analytical techniques. A surface preparation technique to obtain proper contrast of structural defects suitable for QTM analysis was perfected and is now being used routinely.

SECTION II

INTRODUCTION

The objective of this work is to gain fundamental understanding of the role of structural imperfections and chemical impurities on solar cell performance.

The type, density, distribution, and electrical activity of such defects have significant effects on solar cell performance. Most of the processes designed to produce silicon crystals at low cost introduce a high density of defects in crystals, which have a distinct effect on solar cell efficiency.

The types of defects present in many of the low - cost silicon " sheets", produced by a variety of methodology, run the gamut from point defects to dislocations, planar defects such as twins and stacking faults, high and low angle grain boundaries, and second phase inclusions. The types of imperfections present and their density are a function of the specific method used for producing the silicon sheets.

In general, rapidly grown ribbon - type crystals produced by techniques such as the EFG process, the Web Dendritic method, etc., typically contain a relatively high population of dislocations usually arrayed along linear boundaries, a high density of twins, and chemical impurities in the form of precipitates. Sheets formed by slicing of cast crystals, such as SEMIX material, are generally polycrystalline in nature with grain diameters from a fraction of a millimeter to several millimeters, and twin boundaries oriented in different direction within many of the grains.

Quantitative analysis of surface defects was performed by using a Quantimet Quantitative Image Analyzer (QTM 720). The results were double checked by manually counting all the defects. The QTM 720 can differentiate and count 64 shades of grey levels between black and white contrasts. In addition, it can characterize structural defects by measuring their length, perimeter, area, density, spatial distribution, frequency distribution (in any preselected direction), and is programmable in these measurements. However, the QTM 720 is extremely sensitive to optical contrasts of various defects. Therefore, to obtain reproducible results, the contrasts produced by various defects must be similar and uniform for each defect types along the entire surface area of samples to be analyzed. To achieve this contrast uniformity, a chemical cleaning and polishing procedure was developed and perfected for the SEMIX samples described in this report. The cleaning and polishing procedure produced a very clean and even surface. Statistically significant quantitative data was measured and their significance is discussed.

ADVANTAGE OF QUANTITATIVE MICROSCOPY TECHNIQUE

There is significant advantage in using quantitative microscopy technique as described herein to analyze structural defects. Techniques such as transmission electron microscopy (TEM), scanning electron microscopy (SEM), while providing useful information, are usually performed at higher magnifications. For example, TEM analysis is usually carried out in the magnification range 10,000X to 300,000X. Because of the high magnification employed, the area of the field of view is very very small

compared to the total surface area of the starting sample, such as a 2cm by 2 cm sample. Hence, the information obtained,although impressive,may not be statistically significant. However, in our quantitative microscopy technique as used in this report, the magnifications used are very low such as 100X to 1000X. In addition, a total of 62 fields was analyzed from a 2 cm by 2 cm sample. For grain boundary and twin boundary measurement, the total area analyzed was 1.49 cm^2 for a 2 cm by 2 cm sample i.e., a whopping 75% of total surface area was actually measured. For precipitate particles, the total area analyzed was 0.09 cm^2 i.e., 2.3% of the total surface area was measured. For dislocation pits, the total area measured was 0.33% of the total sample area. By way of comparision, if we were to analyze 62 fields from a 2 cm by 2 cm sample by TEM technique at 100,000X, the total area measured will be only 0.00000147 cm^2 which is 0.000147% of the sample surface area.

Therefore, the results obtained by quantitative microscopy technique as described in this report are statistically more significant and reliable than any other technique such as TEM, SEM, etc.

SECTION III

EXPERIMENTAL PROCEDURE

A. CHEMICAL POLISHING AND ETCHING

Eight (8) samples from SEMIX's Ubiquitous Crystalline Process (UCP) Ingot 5848 - 13C were received by Materials Research, Inc., (MRI) from JPL for characterization of structural defects. These samples measured 2 cm by 2 cm and were designated by JPL as A-13, B - 2, C - 12, D - 8, E-13, F - 2, G - 12, and H - 8. These samples were originally fabricated into solar cells by Optical Coating Laboratory, Inc. (OCLI). JPL then stripped the junctions off, mechanically polished these samples, and sent them to MRI for characterization.

The QTM 720 apparatus is extremely sensitive to contrasts produced by various structural defects. It can distinguish 62 shades of grey levels between black and white. By remembering the exact shade, the QTM 720 is able to correctly count each defect types. Therefore, to obtain accurate and reproducible results it is very important that each structural defect type be etched to identical contrast. MRI has now perfected a chemical cleaning, polishing, and etching procedure to produce contrasts to such a demanding requirement in these Semix samples. All chemicals used were Low Sodium MOS, Electronic Grade. The following procedures were used:

1) Grease, Dust and other Surface Contamination Removal

	time (min.)
a. Sample immersed in trichloroethylene	3
b. Sample rinsed in acetone	3
c. Sample rinsed in 2- Propanol	3
d. Compressed N_2 gas to blow off 2 - Propanol to prevent stain marks	0.5

2) Protective Coating Application

a. Using a fine paint brush, Apiezon Wax dissolved in trichloroethylene was applied to one surface of the silicon sample.

b. The wafer was then heated on a hot plate to about 120° C to accelerate evaporation of trichloroethylene. The Apiezon Wax melted and spread uniformly covering the entire surface. All of the trichloroethylene evaporated leaving behind a thin coating of the acid - resistant Apiezon Wax covering the surface.

3) Silicon Oxide Layer Removal

	time (min.)
a. Sample was immersed in concentrated HF	4
b. It was then rinsed in distilled water	4
c. It was then rinsed in 2-propanol	4
d. N_2 gas to blow off excess 2-propanol	0.5

The protective coating application is done for two reasons: i) to prevent attack and dissolution of samples from two surfaces. By using a wax coating, the coated surface is prevented from chemical attack during polishing and etching procedure, ii) the protective coating may be dissolved later in trichloroethylene and JPL may in future build a solar cell on that surface. Thus a direct correlation between cell efficiency and defect densities for each sample may be obtained.

4) Chemical Polishing Procedure

The chemical polishing solution is a mixture by volume of 1 part nitric acid (HNO_3) : 2 parts hydrofluoric acid (HF) : 3 parts acetic acid (CH_3COOH). The following procedure was used :

	time (min.)
a. The wafer was immersed at 50 $\pm$ 3° C in polishing solution	0.1-0.75
b. It was then rinsed in deionized distilled water	4
c. It was then rinsed in 2 - propanol	4
d. N_2 gas blown to dry sample surface	0.5
e. Sample was observed under micrscope and polishing was continued until a smooth flat surface was observed	0.1-0.75

5) Chemical Etching Procedure

The chemical etching solution consists of 2.5 gm. of chromium trioxide (CrO_3) dissolved in 15 ml. deionized distilled water

and 15 ml. concentrated hydrofluoric acid (HF). The following procedure was used:

	time (min.)
a. Sample was immersed in the chemical etching solution	0.1-0.3
b. It was then rinsed in deionized distilled water	4
c. It was then rinsed in 2 - propanol	4
d. N_2 gas blown to dry sample surface	0.5
e. Sample was observed under microscope and etching procedure was continued until dislocation pits are visibly observed	

The etching times for the Semix samples were as follows.

Sample No.	Etching Time (Sec.)
A-13	67
B-2	60
C-12	48
D-8	37
E-13	77
F-2	82
G-12	61
H-8	48
Average	60

SECTION IV

RESULTS AND DISCUSSION

A. MEASUREMENT OF GRAIN BOUNDARIES, TWIN BOUNDARIES, PRECIPITATE PARTICLES, AND DISLOCATION PITS

Using an Olympus Inverted Optical Metallurgical Microscope, Model PME , approximately 62 fields on each sample were analyzed for structural defects. Figure 1 shows the relative positions of the 62 fields that were observed on each sample. The feature under investigation is counted in each field and averaged over the 62 fields for a statistical average of the overall sample. The field of view of the microscope is a necessary quantity to know so that some dimensions can be given to the defect feature. Using a 0.01 cm - 0.001 cm calibrated standard microscope slide, the diameter of the field of view was measured at different magnifications. From this data, the circumference and the area of the field of view was determined. This data is tabulated in Table 1. Table 1 shows that as the magnification approximately doubles for successive objective setting, the diameter of field of view decreases by about half.

The defect measurements were done in three (3) separate steps. First, the grain boundary and twin boundary intersections were

measured for all the 62 fields using a magnification of 100X in the polished condition. Next, the precipitate particles were measured for all the 62 fields using a magnification of 400X in the polished condition. Next, the sample was etched in the etching solution and immediately measurements were made for dislocation pits for all the 62 fields at a magnification of 1000X.

All of these measurements were made manually. Attempts were made to use the Quantitative Image Analyzer (Quantimet QTM 720). However, this was not successful since the contrast on the CRT was poor for the fine precipitates at 1000X. These manual measurements were done very carefully, the measurements were repeated, and found to be reproducible. All measured data is listed in Appendix.

1) Measurement of Grain Boundary and Twin Boundary Length Per Unit Area

Since grain boundaries can be location of efficient carrier recombination centers and act as sinks for impurities which can be detrimental to the efficiency of the solar cell,[1-4] the grain boundary length per unit area is an important quantity to know. Using a statistical method of counting the intersections of the grain boundaries and twin boundaries with a test line, the length per unit area can be calculated using the following relationship[5,6] :

$L_A = (\pi/2) \cdot P_L$, where

L_A = line length of grain boundaries or twin boundaries per unit area (cm / cm^2)

P_L = number of point intersections of grain boundaries or twin boundaries per unit length of test lines.

Figures 2, 6, 7, 8, 9, 12, 14, 16, and 17 show typical structures of twin boundaries and/or grain boundaries in the Semix samples. The Appendix Tables 1, 4, 7, 10, 13, 16, 19, and 22 contain a listing of the raw measured data for grain boundaries and twin boundaries. The information in the above tables has been summarized in Table II, along with calculated values for arithmetic mean and standard deviation.

Several tentative graphs are shown in order to determine any apparent relationship in the measured data. These graphs are preliminary and subject to revision as more and more samples are examined and better information about sample history is obtained from other sources (such as Semix Corporation, JPL, OCLI, etc.,). Figure 20 shows a plot of twin boundary length as a function of the distance of the wafer from top of the ingot. Figure 20 shows that, as a first approximation, twin boundary density (expressed as length/unit area) decreases as the distance from top of ingot increases. Samples A and E located at top of the ingot have the highest densities. To explain this phenomenon, data on crystal growth conditions are required. Figure 24 is a plot of the data listed in Table II. As a first approximation, Figure 24 shows that as the grain boundary length/unit area increases, the twin boundary length/unit area increases rapidly at first then levels off and decreases. To explain this

observation, as the grain size decreases the grain boundary length/unit area increases. If on the average, the same number of twin boundaries were still present in the now-smaller grains, then the number of twin boundaries will also increase with a corresponding increase in twin boundary length/unit area. The dotted curve in Fig. 24 shows this trend.

2) Measurement of Precipitate Particles

The polished samples were observed at a magnification of 400X and the number of precipitate particles were counted in each field. There appeared to be two fairly distinct sizes of what was counted as precipitate particles. The large - sized defects were clearly recognized to be precipitate particles. However, there were smaller features, that could not be resolved clearly, which looked like precipitate particles. The only other possibilities were that these features are small stain marks or etch pits. Since there is some questions as to the identity of these features, observation of these samples at a higher magnification using a Scanning Electron Microscope (SEM) will be performed later. However, for the time being, these features will be regarded as small precipitates subject to correction later. The Appendix Tables 2, 5, 8, 11, 14, 17, 20, and 23 contain a listing of the raw measured data for precipitate particles in these Semix samples. The information contained in the above tables have been summarized in Table III, along with calcu- values for arithmetic mean and standard deviation. Small and large precipitate particle densities are listed separately in Table III.

A sample calculation for small precipitate density in sample F-2 in Table III is shown below:

Magnification = 400X

Area of field = 0.00149 cm^2

$$\overline{X} \text{ for small precipitate} = \frac{447}{62} = 7.2$$

$$\frac{\text{No. of small precipitates}}{\text{unit area}} = \frac{\text{(total no. of small precipitates counted)}}{\text{(total no. of fields) (area of a field)}}$$

$$= \frac{(447)}{(62)\,(0.00149\ cm^2)} \text{ (see Appendix Table 17)}$$

$$= 4.8 \times 10^3 \text{ precipitates/cm}^2$$

Figures 3, 4, 5, 13, and 15 show precipitate particles on some of the Semix samples. The large precipitates are of the order of magnitude $\sim 2 \times 10^{-3}$ cm, while the small precipitates are of the order of magnitude $\sim 5 \times 10^{-4}$ cm and smaller.

3) Dislocation Density

After etching each of the Semix wafers, the dislocation density was determined by counting the number of dislocation etch pits at 1000X in each field of view for approximately 57 fields per sample. The number of fields measured was slightly lower due to mechanical interference of the longer objective lens with the microscope stage. The Appendix Tables 3, 6, 9, 12, 15, 18, 21, and 24 list the raw measured data

for dislocation number density. The information in the above tables have been summarized in Table III, along with calculated values for arithmetic mean and standard deviation. A sample calculation for wafer F-2 in Table III is as follows:

Magnification = 1000X

Total number of dislocation pits counted = 2334 from 59 fields

Area of Field = 0.000238 cm^2

$$\text{Dislocation Pit density} = \frac{\text{(total no. of dislocation pits counted)}}{\text{(total no. of fields) (Area of field)}}$$

$$= \frac{(2334)}{(59)\ (0.000238\ cm^2)} \quad \text{(see Appendix Table 18)}$$

$$= 1.7 \times 10^5 \text{ dislocation pits/cm}^2$$

Figures 10, 11, 18, and 19 show dislocation arrangements in some of the Semix samples.

Figure 21 shows a plot of dislocation density versus large precipitate density from the data listed in Table III (data for small precipitate was not used in Figure 21 since the identity of small precipitate was not positively established). Figure 21 shows that as the large precipitate density increased from sample to sample, the corresponding dislocation density decreased. This trend is quite clear even though some anomalies are present in Figure 21. This observation may be explained on the basis

that dislocation lines constitute tubes of fast diffusion, with a diffusion coefficient close to the coefficient of self diffusion along grain boundaries. The rates of diffusion along such short-circuit paths are significantly higher than for volume diffusion, since the associated activation energies are much lower than for volume diffusion[8]. As the density increases, larger number of short-circuit paths are now available for impurity atoms to migrate. This will result in a decrease in precipitate density. While the intrinsic properties of individual dislocations, dislocation networks, and grain boundaries are governed by the presence of space charge cylinders around defects, the typical electrical response of these structural defects is determined by the presence of impurities in association with the defects. The interaction energy between common impurities such as Fe, Ni, Cu and a dislocation are fairly high, so that impurity atmospheres and impurity precipitates can form at dislocations[9]. When defect intersections occur in crystals, the resulting electrical effects are more pronounced[10, 11]. Presence of impurities at or near crystallographic defects make them electrically active. When P is diffused into the crystals, the impurities from the defects are "gettered" due to reactions between P and impurities decorating the defects. As a result, the defects are no longer electrically active. However, the defects are still present within a diffusion length of beam-generated charge carriers. Hence, predominant electrical effects in silicon devices are caused by defect-impurity association (see Fig. 10, 11, &19).

B. POSSIBLE RELATIONSHIP BETWEEN CELL EFFICIENCY AND DEFECT DENSITY

Table IV lists the defect densities in these Semix samples as obtained by MRI along with the data for cell efficiency and diffusion length as obtained by OCLI[7]. The data for cell efficiency was plotted as a function of the observed data for different types of structural defects. Figure 22 shows a plot of cell efficiency versus twin boundary density. An approximate inverse relationship is observed. The significance of this graph is that the grain boundary substructure may influence cell efficiency in Semix material. In other words, the defect structure within grains may influence the cell efficiency more than the grain boundary itself. Furthermore, as mentioned in page 21, interactions of these substructures with one another and with impurity atmospheres may cause more pronounced electrical effects. It is proposed that MRI verify such effects by obtaining quantitative relationship during next year's effort. For example, MRI should determine what fraction of the total number of each defect types are electrically active. Also, quantitative data is required on total chemical impurities and the distribution of these impurities along the structural defects, cell junction, and cell surfaces. Neutron Activation Analysis is being performed on these samples, and the data will be sent to JPL next week.

C. POSSIBLE RELATIONSHIP BETWEEN DIFFUSION LENGTH AND DEFECT DENSITY

The numerical data for diffusion length was plotted in several ways using the various observed data for different types of structural defects listed in Table IV. Figure 23 shows a graphical plot of diffusion length versus observed dislocation density in the eight samples. The figure shows an important trend. An inverse relationship is observed between diffusion length and dislocation density. Since the average grain size in these samples is expected to be larger than the diffusion length in a single crystal Semix of the same doping level (data not currently available), the effective lifetime and diffusion length in the polycrystalline Semix samples is expected to be reduced by substructures within grains (such as twin boundary density, dislocation density, and precipitate particle density along with chemical segregation around these substructures). It is important that during next year's effort, MRI should generate quantitative information to establish definitive relationship on how diffusion length is influenced by density of structural defects in Semix. A similar study for other silicon materials studied by MRI[12-22] for JPL will result in a fundamental understanding of the various silicon microstructures and substructures and their effect on electrical properties of solar cells.

D. NUMERICAL SIGNIFICANCE OF MEASURED DATA

The measured data for the Semix samples are listed in Appendix Tables 1 thru 24, and the information in these tables are summarized in Tables II, III, and IV. The defect structure characterization was done using a statistical sampling of each sample over a TV raster and from this an average value for each defect type in each sample was obtained.

Among these eight samples, the large precipitate density varied from 65 to 745 per cm^2, while the total (large and small) precipitate density varied from 2.7×10^3 to 23×10^3 per cm^2.

Grain boundary length per unit area varied from 4.5 to 13.8 cm/cm^2, whereas the twin boundary length per unit area varied from 12.2 to 99.0 cm/cm^2. Samples A-13 and E-13 had the higher twin boundary length per unit area, while the grain boundary length per unit area for these samples were in the middle range. Samples C-12, D-8, and G-12 had the higher numerical values for grain boundary length, but in the middle range for twin boundary length. Samples B-2 and F-2 had lower values for both grain boundary and twin boundary length. Figure 24 shows that as the grain boundary length/unit area increases, the twin boundary length/unit area also increases at first rapidly, but at higher values for grain boundary length/unit area, it levels off and gradually decreases.

Dislocation density in these samples varied from 4.9×10^4 to $86 \times 10^4/cm^2$.

Sample A-13 had the lowest dislocation density but highest large precipitate density (see Table IV). Samples C-12, G-12, and H-8 had lower precipitate density but had higher dislocation density. Therefore, an approximate inverse relationship was observed between dislocation density and precipitate density as shown in Figure 21.

Sample A-13 had the highest twin boundary length per unit area as well as the highest large precipitate density. Figures 2 and 3 show some regions in this sample that illustrate this observation.

Figures 4 and 5 show some precipitate particles in fields free of twin boundaries and grain boundaries in sample B-2 . This sample had lower twin boundary and grain boundary lengths per unit area but precipitate density was in the medium numerical value. Figures 6 and 7 show some twin boundary and grain boundary regions in sample C-12. Sample C-12 had higher grain boundary density. Sample D-8 had the highest grain boundary length per unit area and also a relatively high twin boundary density as illustrated in Figures 8 and 9. Figure 10 shows an area in sample D-8 where dislocations have piled up between twin boundaries Figure 11 shows another type of interaction between dislocations and a twin boundary. Such a boundary may be electrically active as discussed in page 21.

Figures 12 and 13 show a higher twin boundary density region, which is typical of sample E-13. Sample F-2 has a lower grain boundary and

twin boundary length per unit area, but a high precipitate density. Figure 14 shows interaction between twin boundary and grain boundary, and Figure 15 shows a region of higher precipitate density in sample F-2. Figures 16 and 17 show sample regions in sample G-12 with typical grain boundary and twin boundary structures. Sample H-8 has the highest dislocation density and typical areas are illustrated in Figures 18 and 19. In Figure 18, the dislocations form simple networks. Figure 19 shows linear arrays of dislocations interacting with twin boundaries on either side

The standard deviation from the mean for all of the defect types is of the same order of magnitude as the mean itself. This shows that there is a large variation in the distribution of defects from one field to another in the same sample.

SECTION V

CONCLUSIONS

A chemical surface preparation technique to obtain proper contrast of structural defects suitable for QTM analysis of Semix samples was perfected, and is now being routinely used. Statistical quantitative techniques were applied to these samples with a good degree of confidence.

The samples examined had two distinct sizes of precipitate particles. The larger size particles were clearly identifiable (Fig. 4) and had diameters about $2X\ 10^{-3}$ cm and larger. The smaller surface iregularities, which appeared like precipitates had sizes $5\ X\ 10^{-4}$ cm and smaller. The smaller irregularities will be analyzed further to confirm that they are indeed precipitates.

The measured data indicated several important trends. The twin boundary density (expressed as length/unit area) decreases as a function of the distance from top of the ingot (Fig. 20). The dislocation density exhibited an inverse trend with respect to the large precipitate density(Fig. 21 and Table III). An approximate inverse relationship was observed between cell efficiency versus twin boundary density(Fig. 22). The significance of such a relationship is that the grain boundary substructure may influence cell efficiency in Semix material more

than grain boundary itself. An approximate inverse relationship was was observed between diffusion length and dislocation density (Fig. 23 and Table IV). The twin boundary density varied from 2 to 12 times the corresponding grain boundary density. Figure 24 shows that as the grain boundary density increases, the twin boundary density increases rapidly at first, then levels off, and gradually decreases.

While the intrinsic properties of individual dislocations, dislocation networks, and grain boundaries are governed by the presence of space charge cylinders around defects, the typical electrical response of these structural defects is determined by the presence of impurities in association with the defects. The interaction energy between common impurities such as Fe, Ni, Cu, etc., and a dislocation are fairly high, so that impurity atmospheres and impurity precipitates can form at dislocations. When defect intersections occur in crystals (Fig. 10, 11, & 19), the resulting electrical effects are more pronounced.

Quantitative Microscopy observation gives data which is statistically more significant than data obtained from other types of microanalysis such as TEM, SEM, etc.

SECTION VI

REFERENCES

1. K. V. Ravi, Imperfections and Impurities in Semiconductor Silicon, John Wiley & Sons, New York, 1981.

2. Z. C. Putney and W. F. Regnault, Solar Cells, vol. 1, No. 3, p. 285-292, May, 1980.

3. G. H. Schwuttke, T. F. Ciszek, and A. Kron, "Silicon Ribbon Growth by a Capillary Action Shaping Technique", Final Report, DOE/JPL 954144, IBM Corporation, Hopwell Junction, New York, 1977.

4. B. L. Sapori and A. Baghdadi, Solar Cells, vol. 1, No. 3, p. 237-250, May, 1980.

5. E. E. Underwood, Quantitative Stereology, Addison-Wesley Publishing Company, Reading, Massachusetts, 1970.

6. E. E. Underwood, Metals Handbook, vol. 8, p. 37-47, American Society for Metals, Metals Park, Ohio, 1973.

7. P. A. Iles and D. C. Leung, "Silicon Solar Cell Process Development, Fabrication, and Analysis", 26th Monthly Report, JPL 955089, Optical Coating Laboratory, Inc., City of Industry, California, October, 1981.

8. J. Friedel, Dislocations, p. 290-292, Addison-Wesley Publishing Company, Reading, Massachusetts, 1964.

9. A. D. Kurtz, S. A. Kulin, and B. L. Averbach, Phys. Rev., vol. 101, p. 1285, 1956.

10. H. B. Serreze, J. C. Swartz, G. Entine, and K. V. Ravi, Mater. Res. Bull., vol. 9, p. 1421, 1976.

11. G. H. Schwuttke, T. F. Ciszek, and A. Kran, "Silicon Ribbon Growth by a Capillary Action Shaping Technique", Quarterly Report No. 6, DOE/JPL 954144, IBM Corporation, Hopwell Junction, New York, Dec. 15, 1976.

12. R. Natesh, H. A. Qidwai: "Quantitative Analysis of Defects in Silicon", One - Time Report on Crystal Etching Preparation Technique, DOE/JPL 954977, Materials Research, Inc., Technical Report: MRI - 259, 1978.

13. R. Natesh, J. M. Smith, T. Bruce, H. A. Qidwai: "Quantitative Analysis of Defects in Silicon", Final Report, DOE/JPL 954977, Materials Research, Inc., Technical Report: MRI - 276, 1980.

14. R. Natesh, J M. Smith: "Quantitative Analysis of Defects in Silicon", Monthly Technical Letter Progress Report No. 10, DOE/JPL 954977, Materials Research, Inc., Technical Report: MRI - 270, 1979.

15. R. Natesh, J. M. Smith, H. A. Qidwai, T. Bruce: "Quantitative Analysis of Defects in Silicon", Quarterly Progress Report, DOE/JPL 954977, Materials Research, Inc., Technical Report: MRI - 273, 1979.

16. R. Natesh, M. Plichta, J. M. Smith: "Analysis of Defect Structure in Silicon", Informal Technical Report, DOE/JPL 955676, Materials Research, Inc., Technical Report: MRI - 280, 1980.

17. R. Natesh, M. Mena, J. M. Smith, M. A. Sellani: "Analysis of Defect Structure in Silicon", Characterization of Silicon - on-Ceramics Material, Informal Technical Report, DOE/JPL 955676, Materials Research, Inc., Technical Report: MRI - 281, 1981.

18. R. Natesh, M. Mena, J. M. Smith, M. A. Sellani: "Analysis of Defect Structure in Silicon", Mobil Tyco EFG Samples, Informal Technical Report, DOE/JPL 955676, Materials Research, Inc., Technical Report: MRI - 282, 1981.

19. R. Natesh, M. Mena, M. A. Sellani: "Analysis of Defect Structure in Silicon", Single Crystal and Polycrystalline HEM Material, Informal Technical Report, DOE/JPL 955676, Materials Research, Inc., Technical Report: MRI - 283, 1981.

20. R. Natesh, M. Mena, J. M. Smith, M. A. Sellani: "Analysis of Defect Structure in Silicon", Characterization of HAMCO and EFG Solar Cells, Informal Technical Report DOE/JPL 955676, Materials Research, Inc., Technical Report: MRI - 284, 1981.

21. R. Natesh, M. Mena, J. M. Smith, M. A. Sellani: "Analysis of Defect Structure in Silicon", Characterization of HEM Solar Cell Material, Informal Technical Report, DOE/JPL 955676, Materials Research, Inc., Technical Report: MRI - 285, 1981.

22. R. Natesh, M. Mena, J. M. Smith, M. A. Sellani: "Analysis of Defect Structure in Silicon", Characterization of Mobil Tyco EFG Sheet Material, Informal Technical Report, DOE/JPL 955676, Materials Research, Inc., Technical Report: MRI - 286, 1981.

TABLE I

The circumference and the field of view on the Olympus Inverted PME Microscope

Eye-piece Lens	Object-ive Lens	Magnifi-cation	Diameter of field of view (cm)	Circum-ference of field of view (cm)	Area of field of view (cm^2)
10X	5X	50X	0.36	1.13	0.102
10X	10X	100X	0.175	0.55	0.0241
10X	20X	200X	0.089	0.28	0.00622
10X	40X	400X	0.0435	0.137	0.00149
10X	100X	1000X	0.0174	0.055	0.000238

Sample Calculation:

Circumference at 50X = πD = (π) (0.36 cm) = 1.13 cm

Area of field of view at 50X = $\frac{\pi D^2}{4}$ = $\frac{\pi (0.36)^2}{4}$ = 0.102 cm^2

TABLE II

Grain Boundary and Twin Boundary Length Per Unit Area for the Semix Samples

SEMIX Sample Number	Grain Boundary Length per unit area (cm/cm^2)	Twin Boundary Length per unit area (cm/cm^2)
A - 13	8.2 $\bar{x}$ = 2.9 σ = 2.0	99.0 $\bar{x}$ = 34.6 σ = 56.5
B - 2	4.5 $\bar{x}$ = 1.6 σ = 2.2	15.8 $\bar{x}$ = 5.6 σ = 9.3
C - 12	13.4 $\bar{x}$ = 4.7 σ = 2.7	31.9 $\bar{x}$ = 11.2 σ = 11.1
D - 8	13.8 $\bar{x}$ = 4.8 σ = 3.2	44.5 $\bar{x}$ = 15.6 σ = 17.1
E - 13	7.1 $\bar{x}$ = 2.5 σ = 2.1	68.5 $\bar{x}$ = 24 σ = 38
F - 2	5.4 $\bar{x}$ = 1.9 σ = 2.6	12.2 $\bar{x}$ = 4.3 σ = 6.8
G - 12	12.1 $\bar{x}$ = 4.2 σ = 2.6	40.7 $\bar{x}$ = 14.3 σ = 15.5
H - 8	9.4 $\bar{x}$ = 3.3 σ = 1.9	35.9 $\bar{x}$ = 12.6 σ = 13.3
Average	9.2	43.6

$$\bar{x} = \text{arithmetic mean} = \frac{\Sigma \text{ features in all fields}}{\text{Total number of fields}}$$

$$\sigma = \text{standard deviation} = \left[\frac{1}{n-1} \sum_{i=1}^{n} (x_i - \bar{x})^2 \right]^{1/2}$$

TABLE III

Precipitate Particle and Dislocation Pit Density for Semix Samples

SEMIX Sample Number	Precipitate Particle Density (particles/cm^2)			Dislocation Pit Density (pits/cm^2)
	small	large	total	
A - 13	22×10^3 $\bar{x} = 33$ $\sigma = 36.5$	745 $\bar{x} = 1.1$ $\sigma = 1.5$	23×10^3	4.9×10^4 $\bar{x} = 12$ $\sigma = 23$
B - 2	19.5×10^3 $\bar{x} = 29.1$ $\sigma = 18.1$	444 $\bar{x} = 0.66$ $\sigma = 0.95$	20×10^3	9.5×10^4 $\bar{x} = 23$ $\sigma = 45$
C - 12	6.2×10^3 $\bar{x} = 9.2$ $\sigma = 7.7$	65 $\bar{x} = 0.1$ $\sigma = 0.4$	6.3×10^3	37×10^4 $\bar{x} = 89$ $\sigma = 62$
D - 8	2.5×10^3 $\bar{x} = 3.8$ $\sigma = 4.0$	152 $\bar{x} = 0.23$ $\sigma = 0.46$	2.7×10^3	10×10^4 $\bar{x} = 24$ $\sigma = 51$
E - 13	9.1×10^3 $\bar{x} = 13.5$ $\sigma = 10.6$	400 $\bar{x} = 0.6$ $\sigma = 0.7$	9.5×10^3	37×10^4 $\bar{x} = 89$ $\sigma = 96$
F - 2	4.8×10^3 $\bar{x} = 7.2$ $\sigma = 10.5$	740 $\bar{x} = 1.1$ $\sigma = 2.1$	5.6×10^3	17×10^4 $\bar{x} = 40$ $\sigma = 111$
G - 12	6.4×10^3 $\bar{x} = 9.6$ $\sigma = 8.0$	140 $\bar{x} = 0.21$ $\sigma = 0.41$	6.6×10^3	45×10^4 $\bar{x} = 108$ $\sigma = 161$
H - 8	9.5×10^3 $\bar{x} = 14.1$ $\sigma = 10.9$	250 $\bar{x} = 0.4$ $\sigma = 0.8$	9.7×10^3	86×10^4 $\bar{x} = 204$ $\sigma = 235$
Avg.	10.0×10^3	367	10×10^3	31×10^4

For precipitate particle density, 2.3% of the total area was measured.

For dislocation pit density, 0.33% of the total area was measured.

TABLE IV

Defect Density, Conversion Efficiency, and Diffusion Length of Semix Samples.

SEMIX Sample number	Large precipitate density (cm^{-2})	Dislocation pit density (cm^{-2})	Grain boundary length per unit area (cm^{-1})	Twin boundary length per unit area (cm^{-1})	Cell efficiency* (%)	Diffusion length* (μm)
A - 13	745	4.9×10^4	8.2	99.0	7.2	53
B - 2	444	9.5×10^4	4.5	15.8	10.0	51
C - 12	65	37×10^4	13.4	31.9	9.7	41
D - 8	152	10×10^4	13.8	44.5	10.8	47
E - 13	400	37×10^4	7.1	68.5	6.2	35
F - 2	740	17×10^4	5.4	12.2	9.6	22
G - 12	140	45×10^4	12.1	40.7	9.5	19
H - 8	250	86×10^4	9.4	35.9	10.7	31

*data as given in reference No. 7.

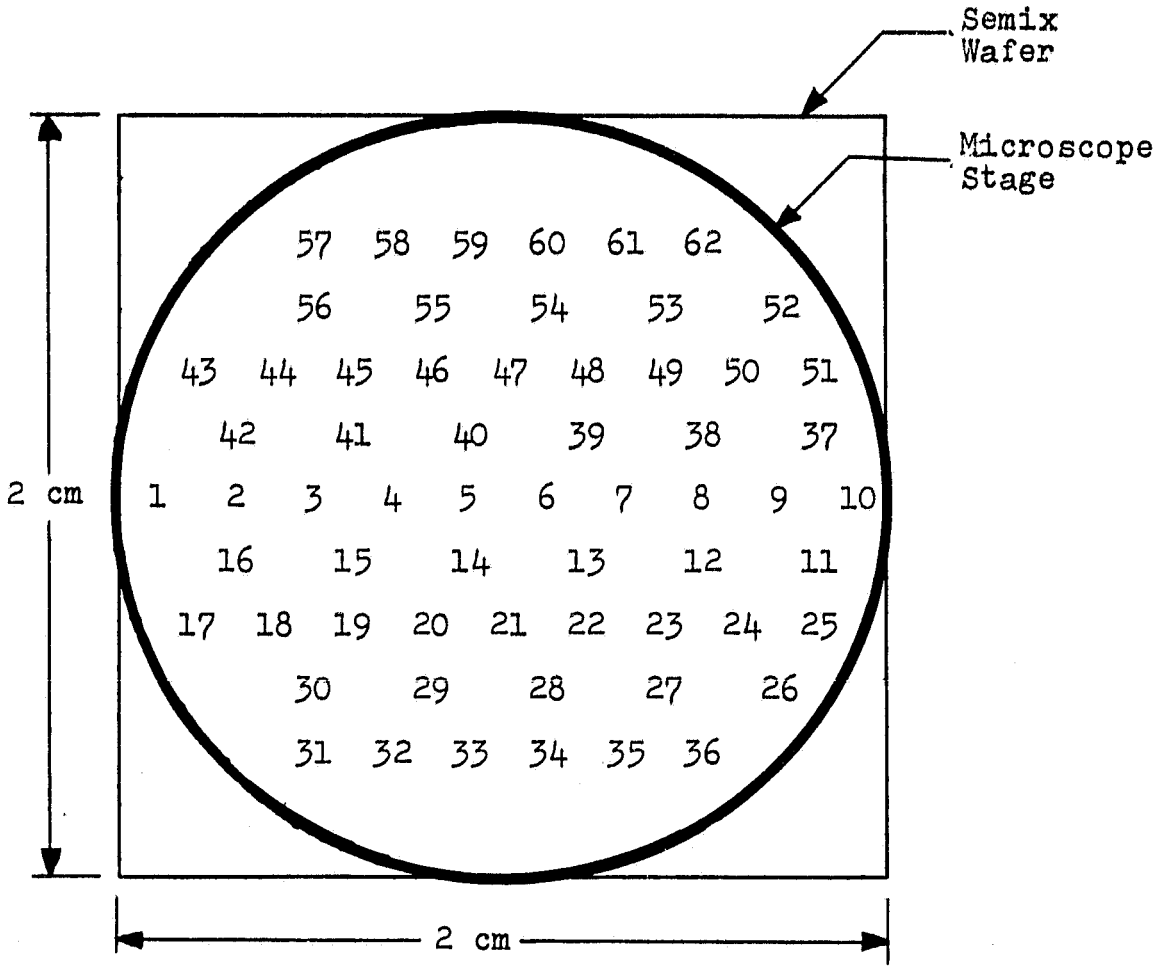

Figure 1. Relative Positions of the Measured Fields on the Semix Wafers.

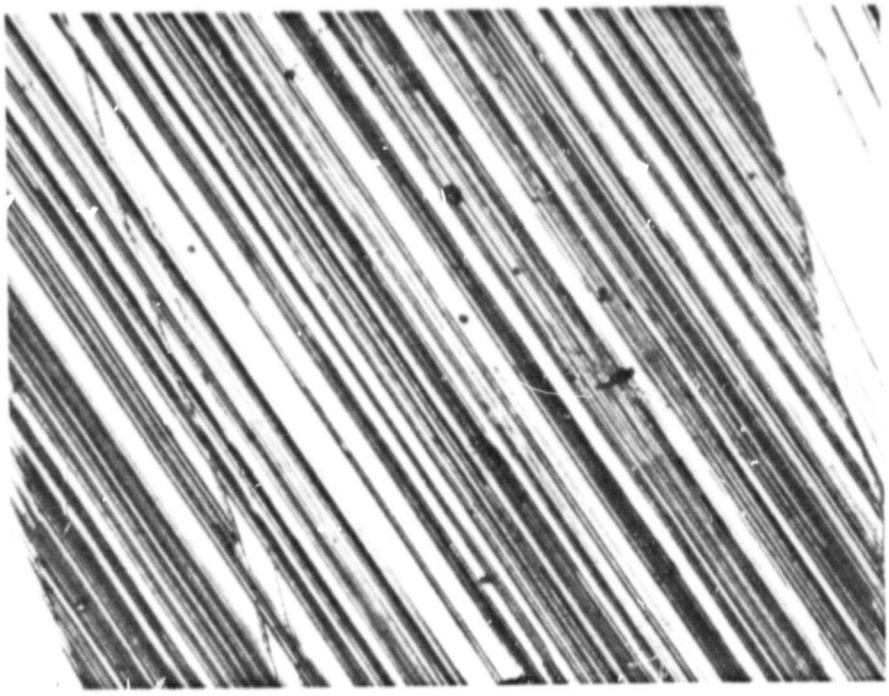

Fig. 2 Region Showing High Twin Density in Semix A-13(50X)

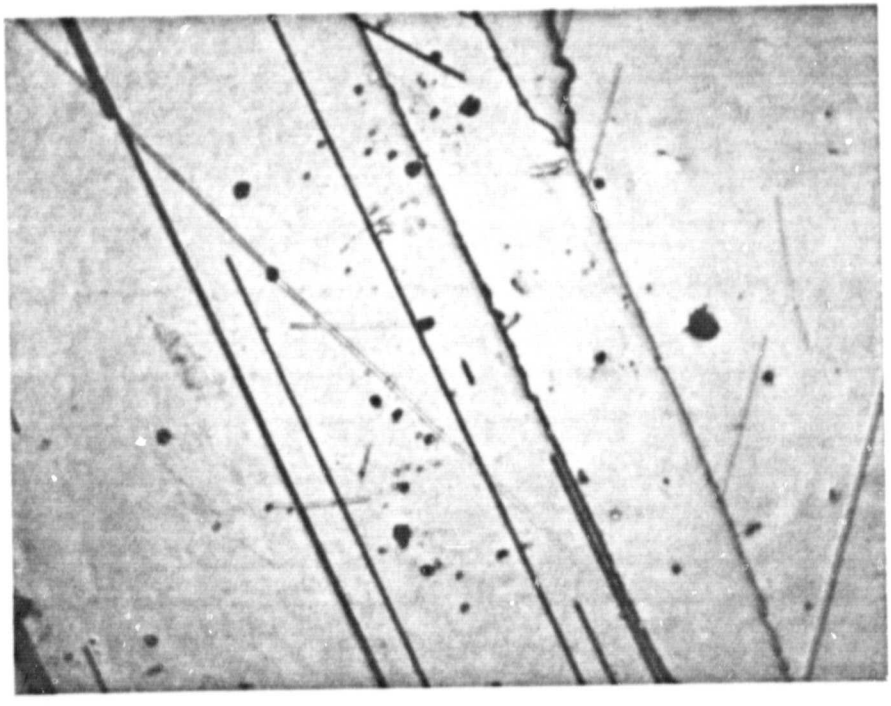

Fig. 3 Region Showing a Large Number of Precipitates in Semix A-13 (50X)

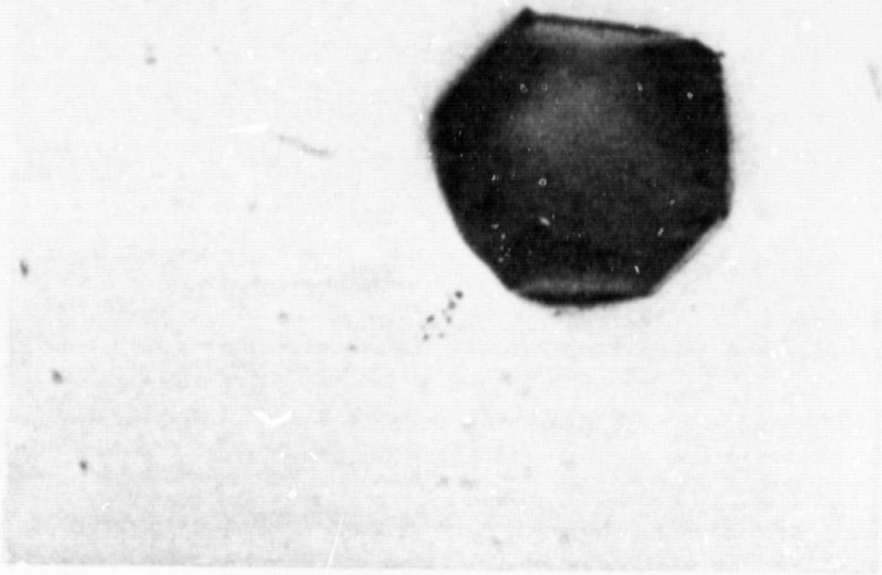

Fig. 4 Large and Small Precipitates in Semix B-2 (1330X)

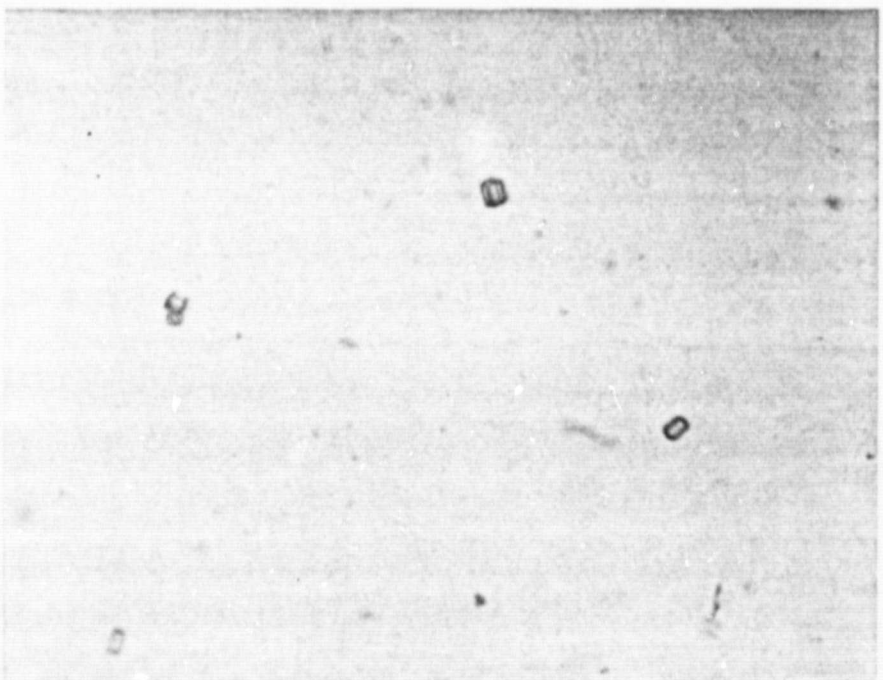

Fig. 5 Precipitates in Semix B-2 (530X)

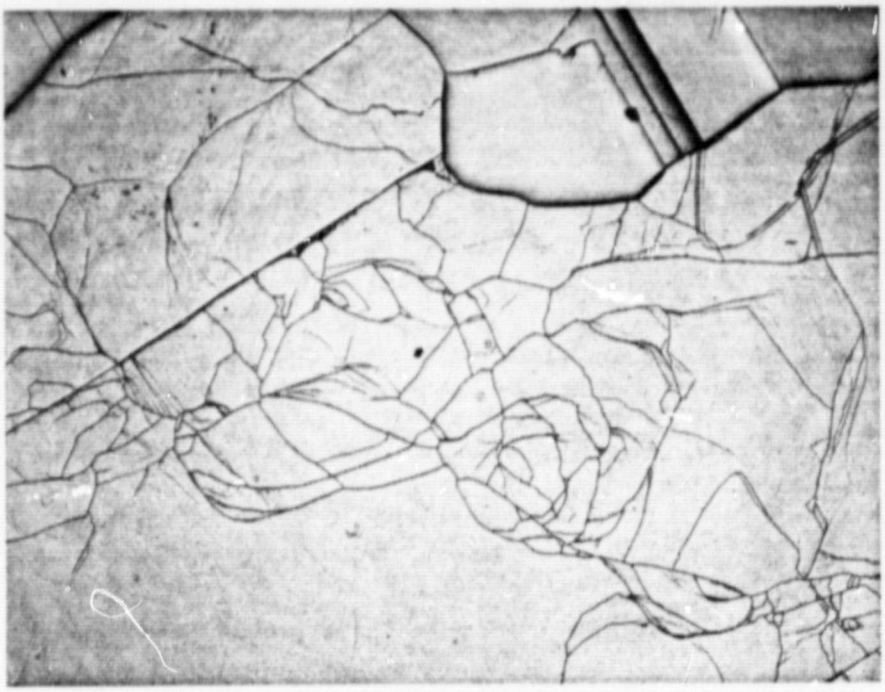

Fig. 6 Many Grains and Grain Boundaries in Semix C-12 (50X)

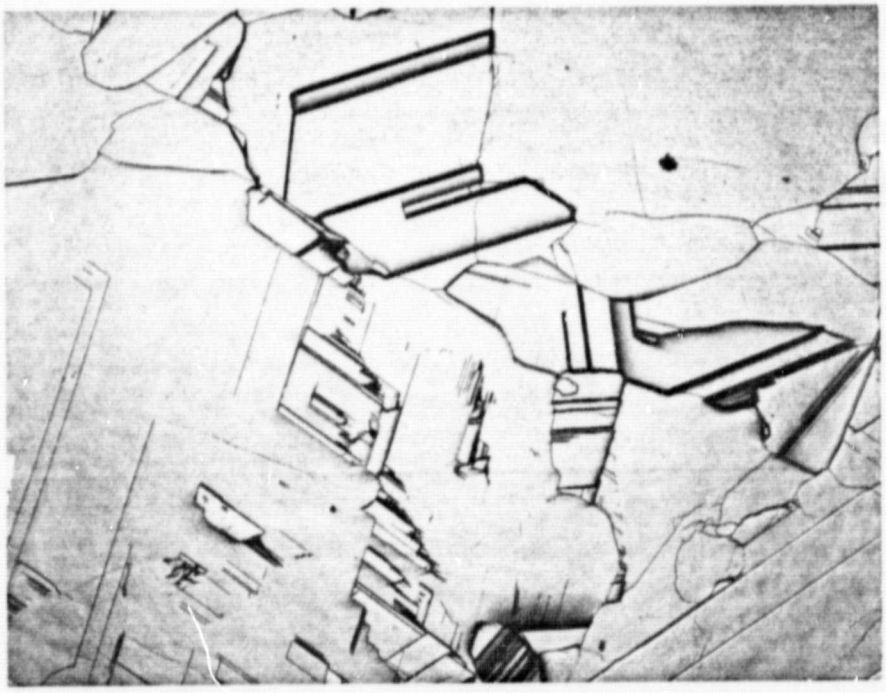

Fig. 7 Twin and Grain Boundaries in Semix C-12 (50X)

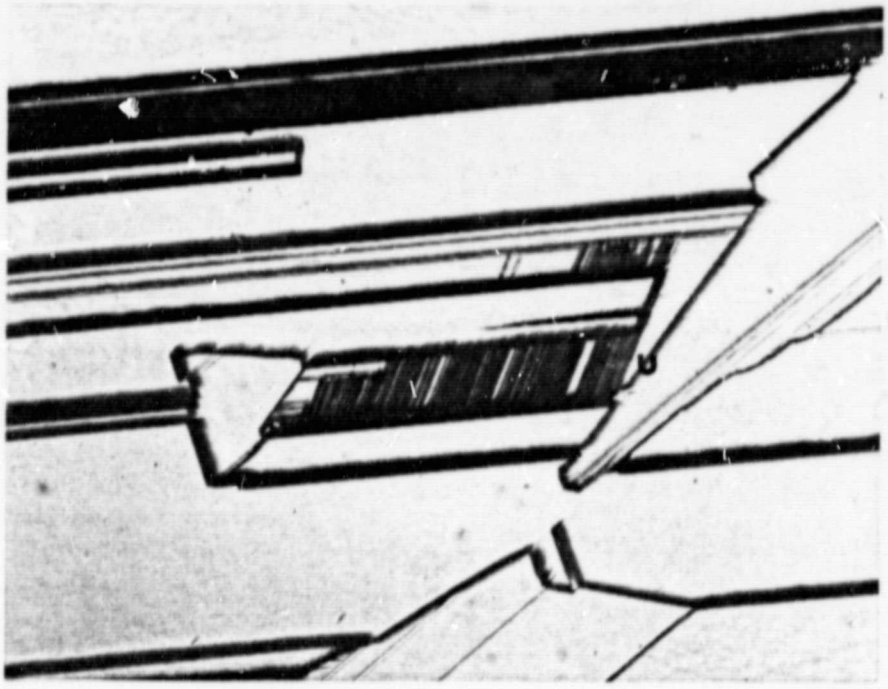

Fig. 8 Large Number of Small Twin Boundaries in Semix D-8. These are not Typical Regions (66X). Region marked "U".

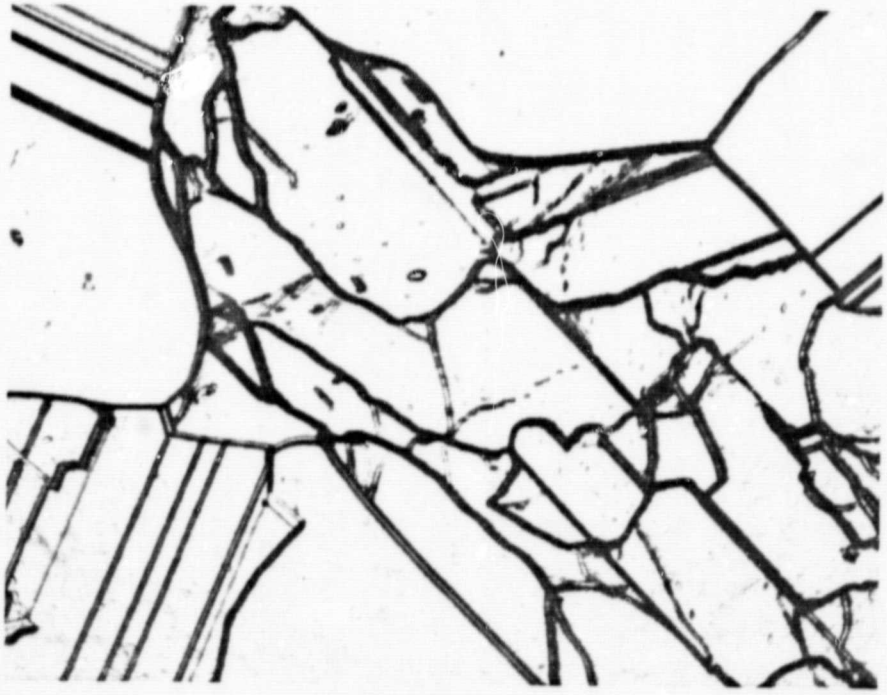

Fig. 9 Many Twin and Grain Boundary Region in Semix D-8 (66X)

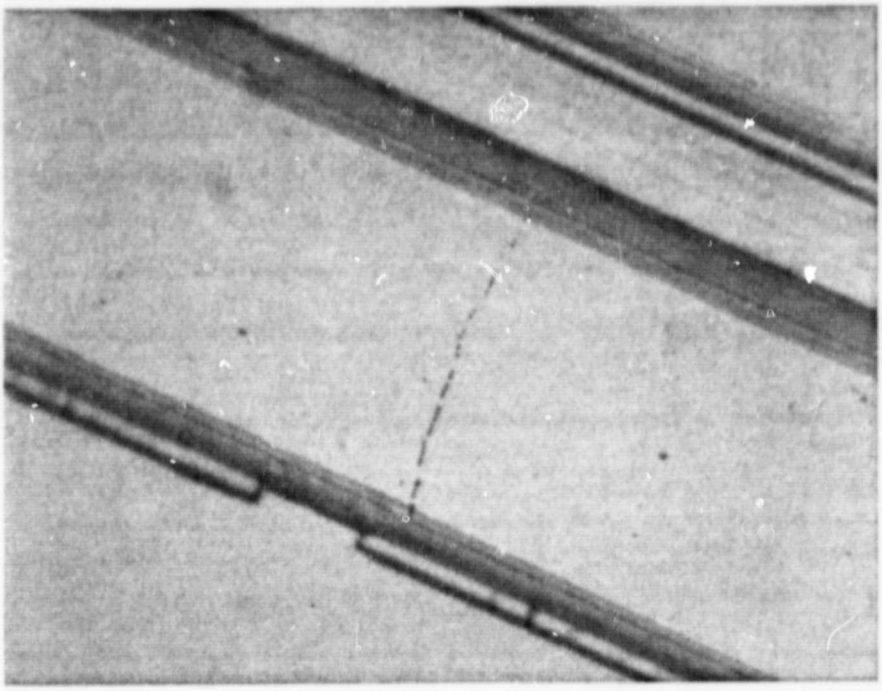

Fig. 10 Dislocations Piled up Between Twins due to Localized Strain in Semix D-8 (600X)

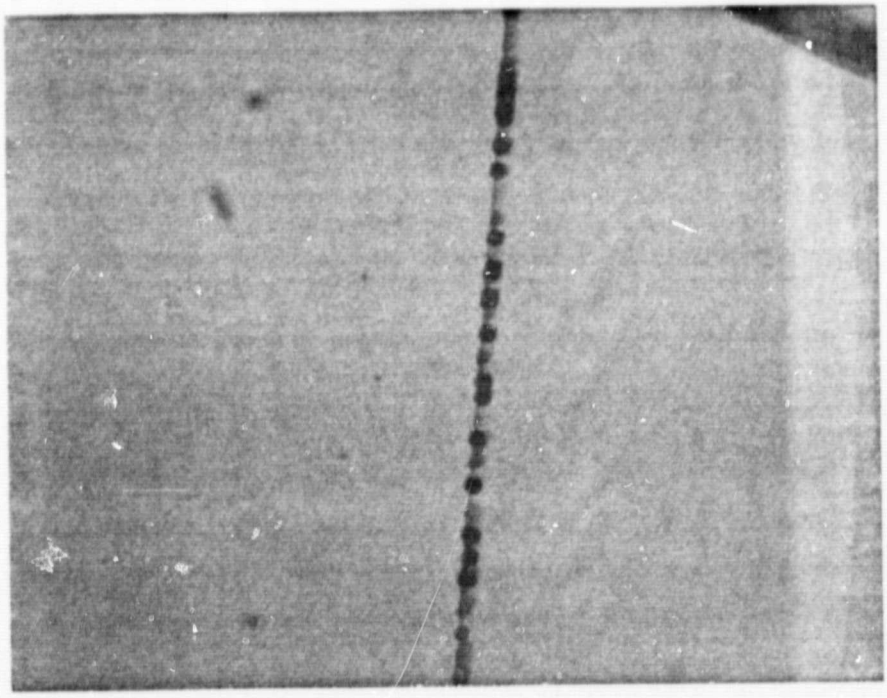

Fig. 11 Dislocations Interacting with a Twin Boundary in Semix D-8 (1500X)

Fig. 12 High Twin Density in Semix E-13 (50X)

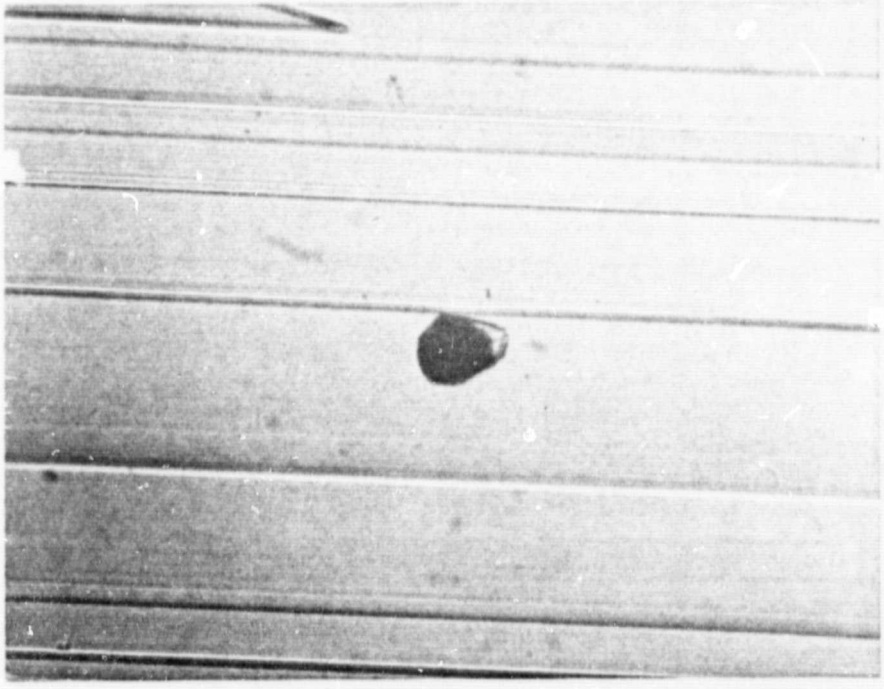

Fig. 13 Large Precipitate Particle Between Twins in Semix E-13 (530X)

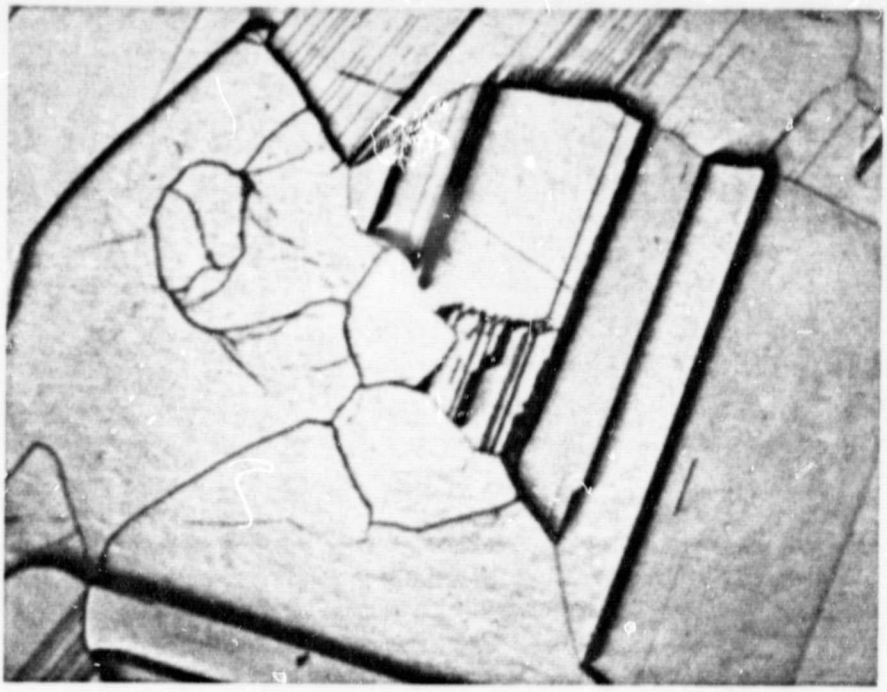

Fig. 14 Twin and Grain Boundary Structure in Semix F-2 (50X)

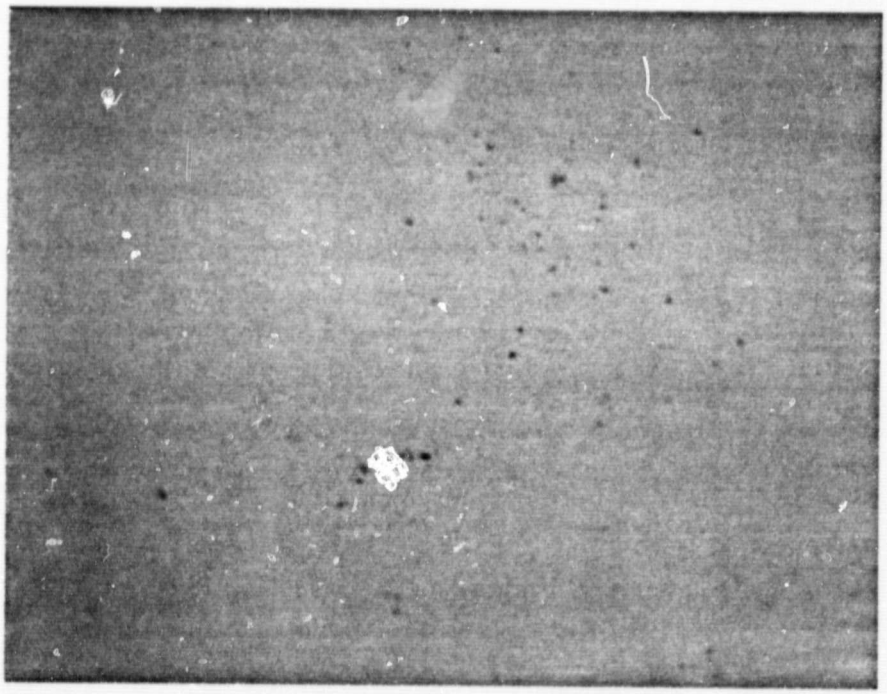

Fig. 15 Small Precipitate Particles in Semix F-2 (200X)

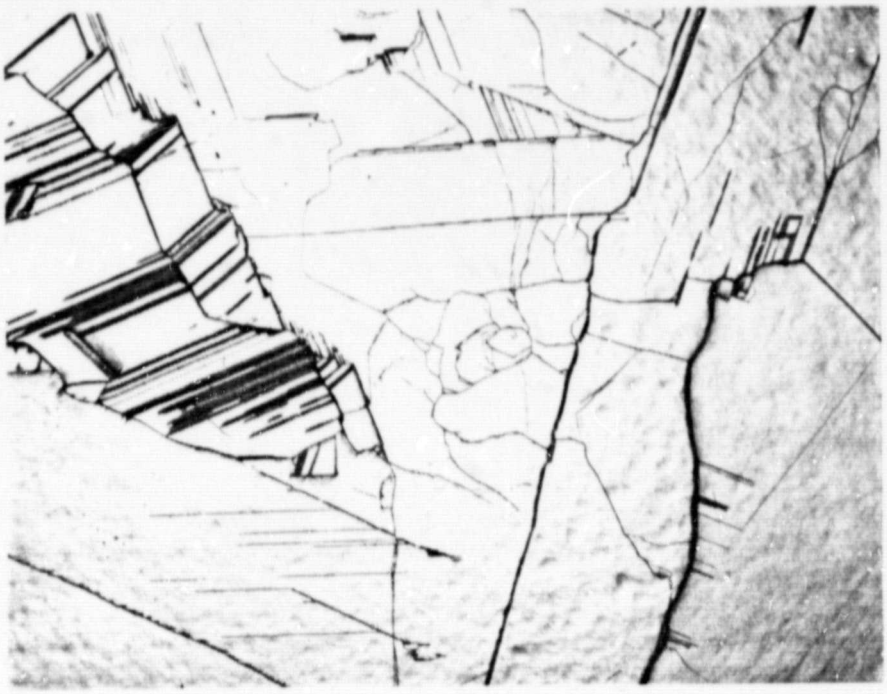

Fig. 16 Twins and Grain Boundaries in Semix G-12 (50X)

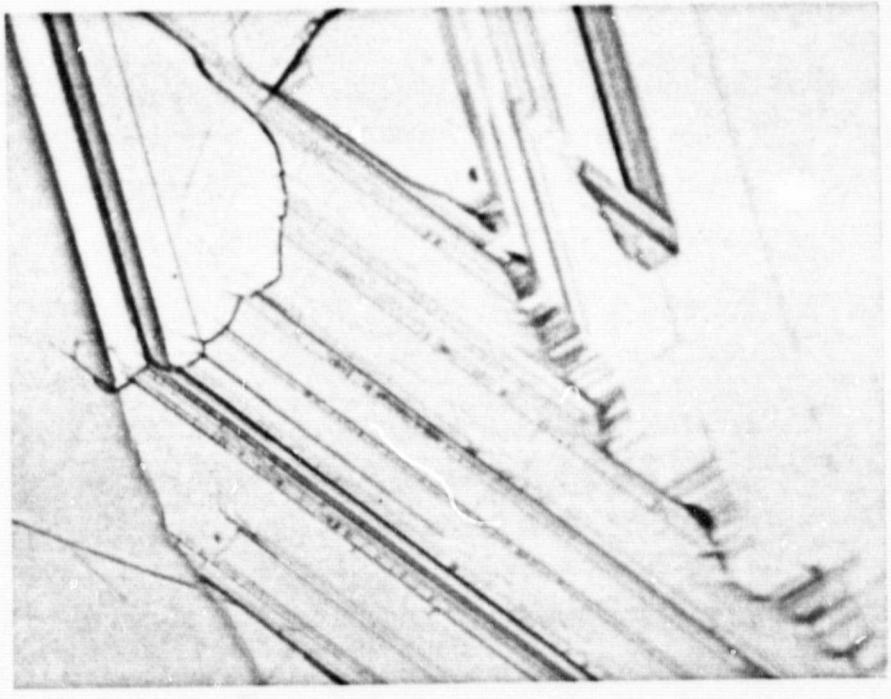

Fig. 17 Region of High Twin Density in Semix G-12 (100X)

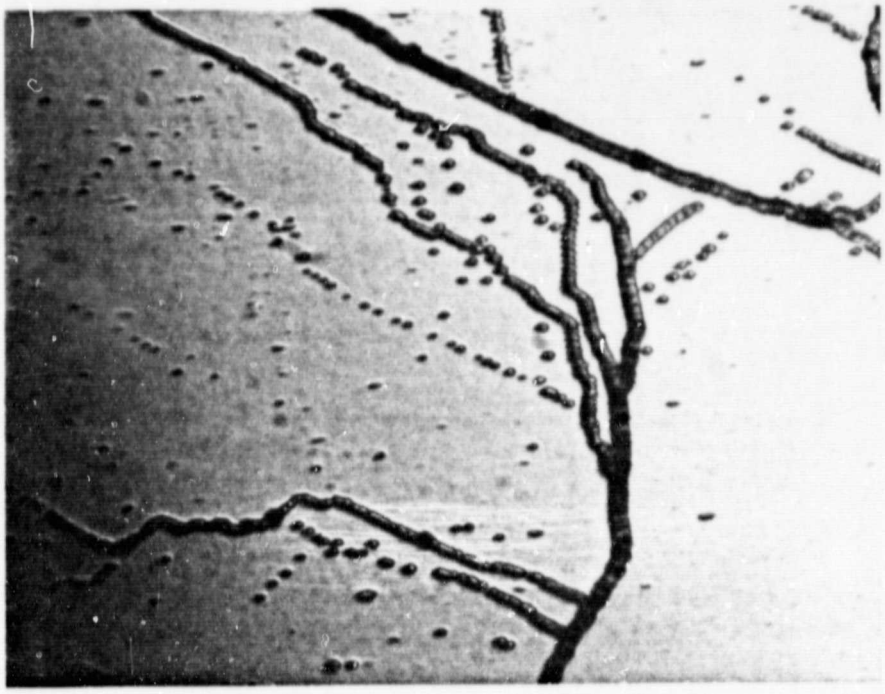

Fig. 18 Dislocation pile-ups in Semix H-8 (1330X)

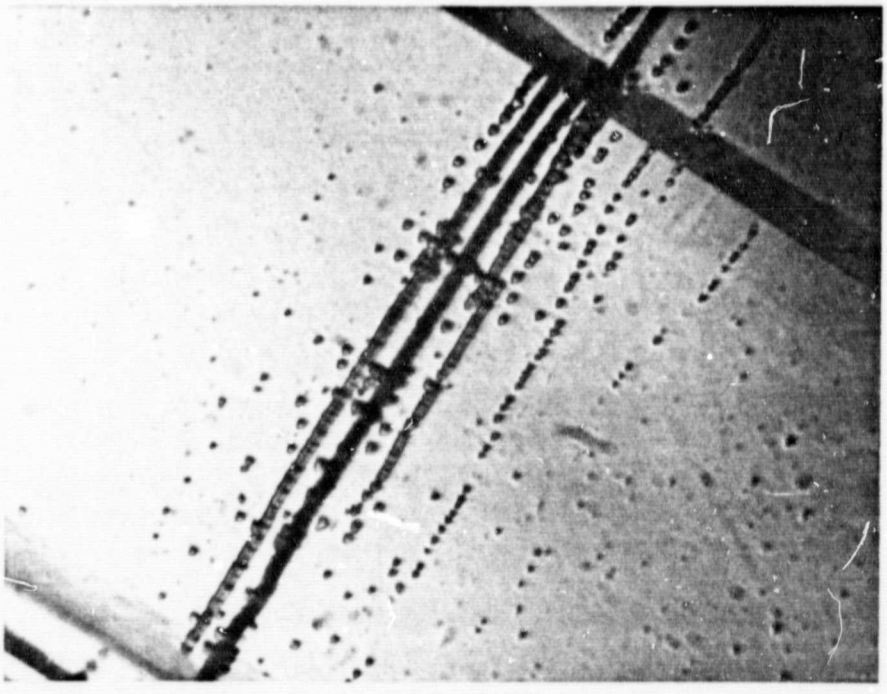

Fig. 19 High Dislocation Density Between Twins in Semix D-8 (1330X)

EXPERIMENT Name Date Period

FIGURE 20

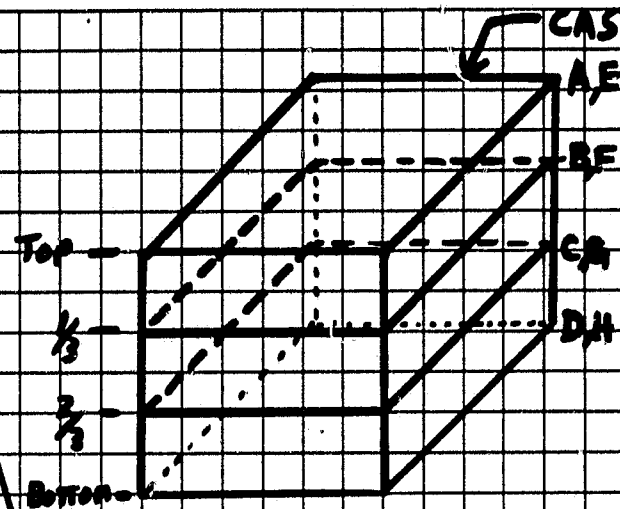

TWIN BOUNDARY LENGTH PER UNIT AREA

VS.

RELATIVE POSITION OF THE WAFER IN THE INGOT FROM THE TOP OF THE SOLIDIFIED INGOT

TWIN BOUNDARY LENGTH PER UNIT AREA (cm/cm^2)

100 90 80 70 60 50 40 30 20 10 0

A E B F G D C H

0 TOP 1/3 2/3 1 BOTTOM

RELATIVE DISTANCE FROM THE TOP OF THE SOLIDIFIED INGOT

EXPERIMENT Name Date Period

FIGURE 21

ORIGINAL PAGE IS OF POOR QUALITY

DISLOCATION PIT DENSITY VS LARGE PRECIPITATE PARTICLE DENSITY

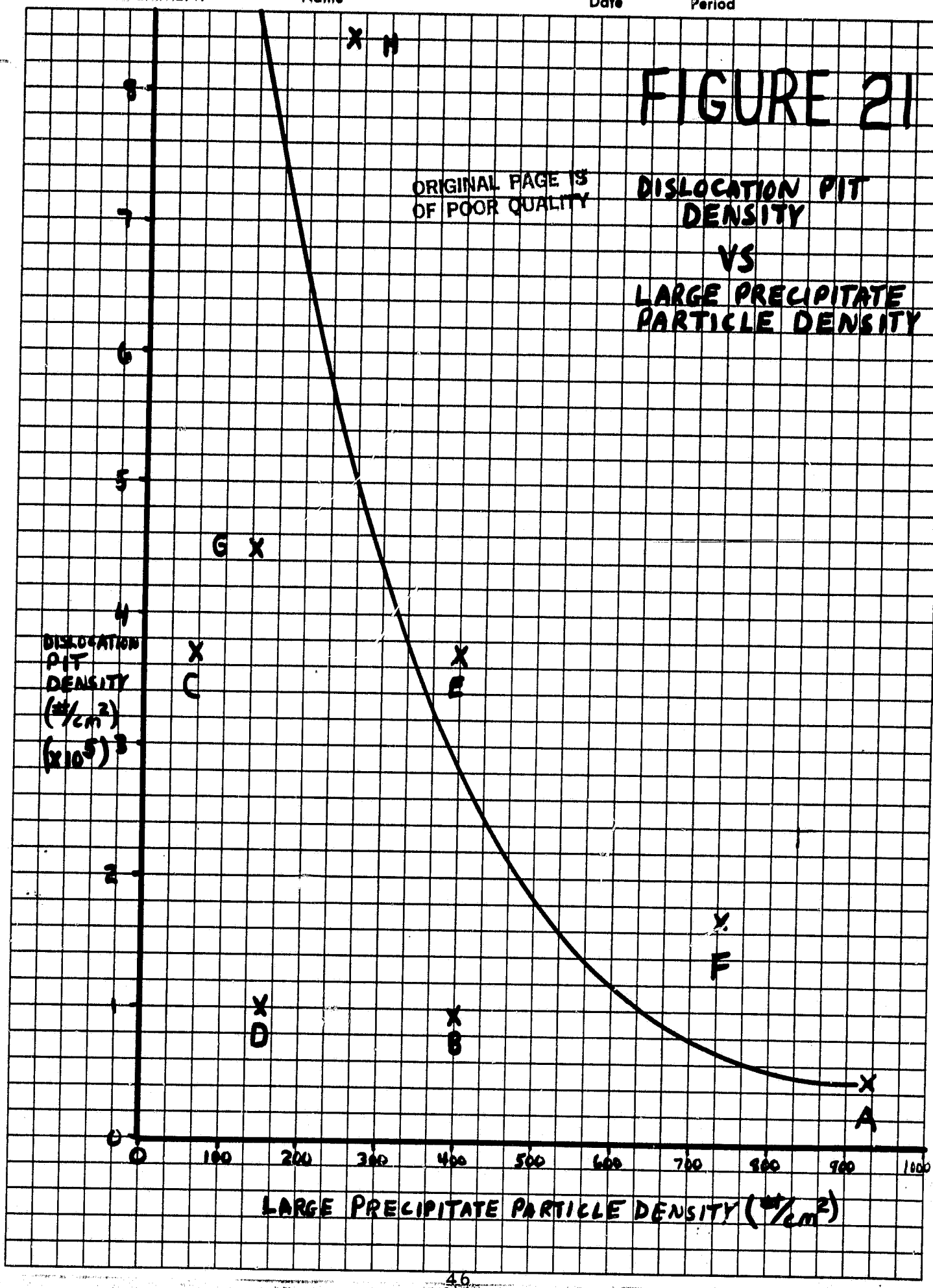

EXPERIMENT Name Date Period

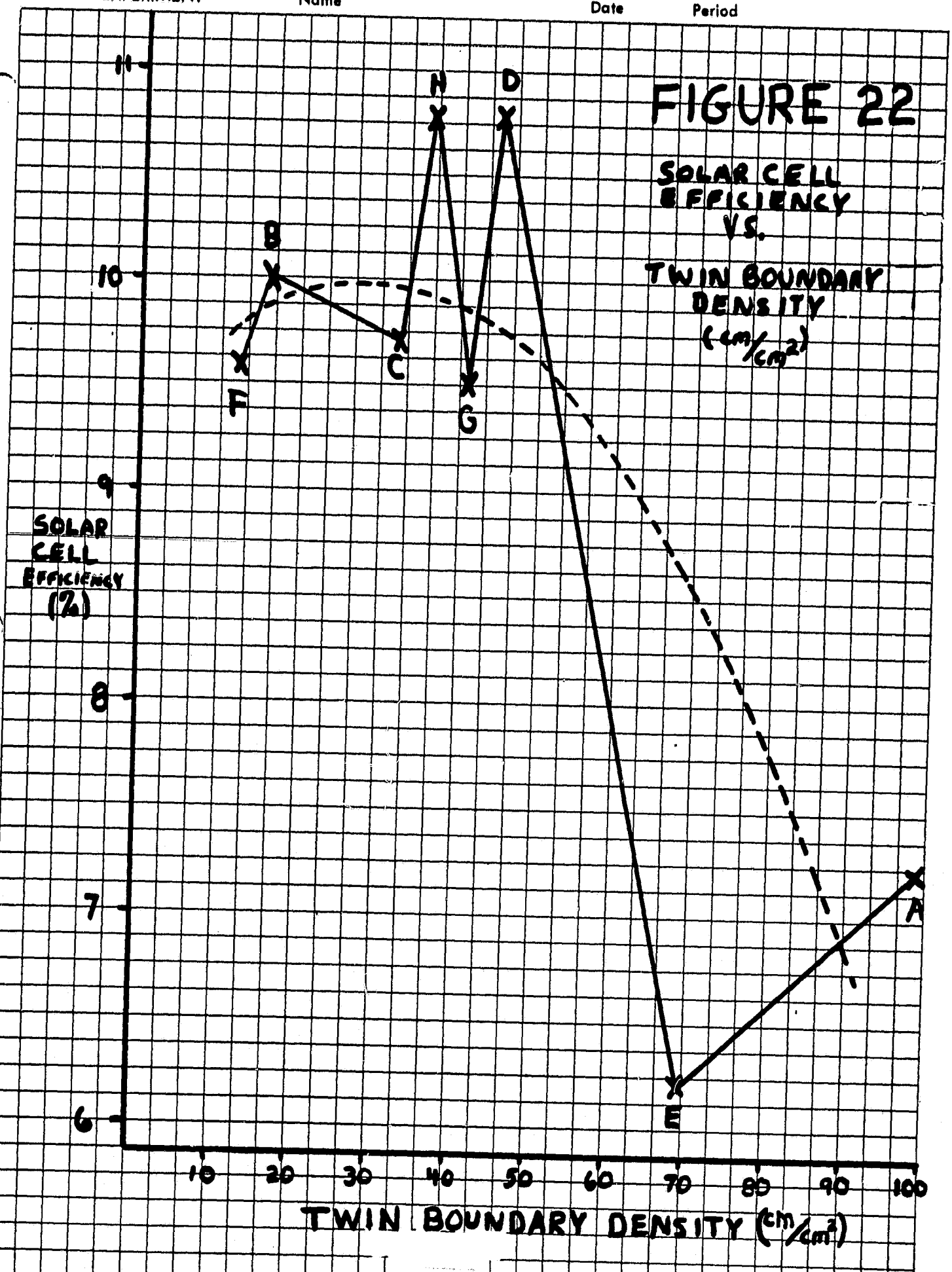

EXPERIMENT Name ORIGINAL PAGE IS OF POOR QUALITY Date Period

FIGURE 23

DIFFUSION LENGTH VS DISLOCATION PIT DENSITY

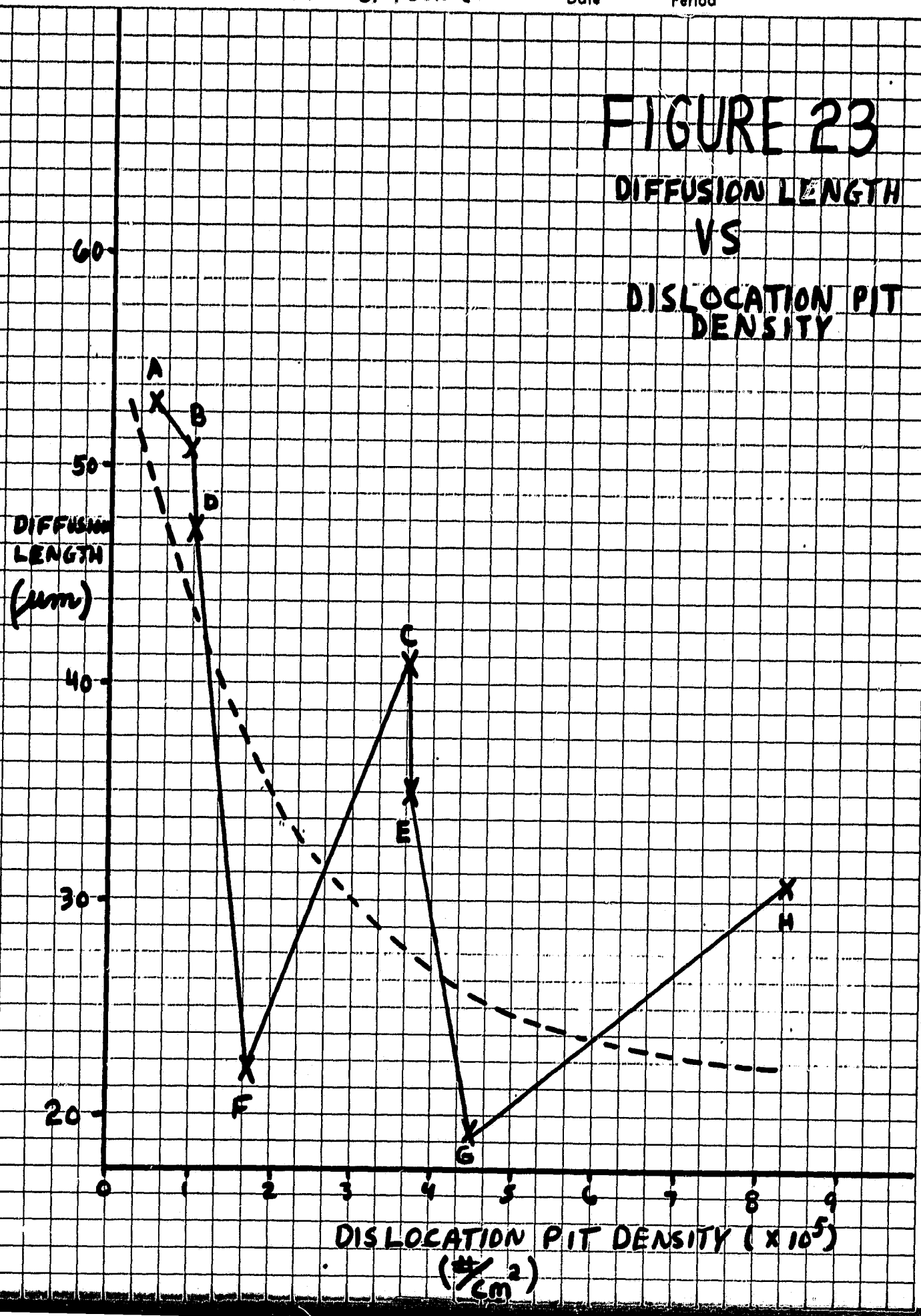

EXPERIMENT Name Date Period

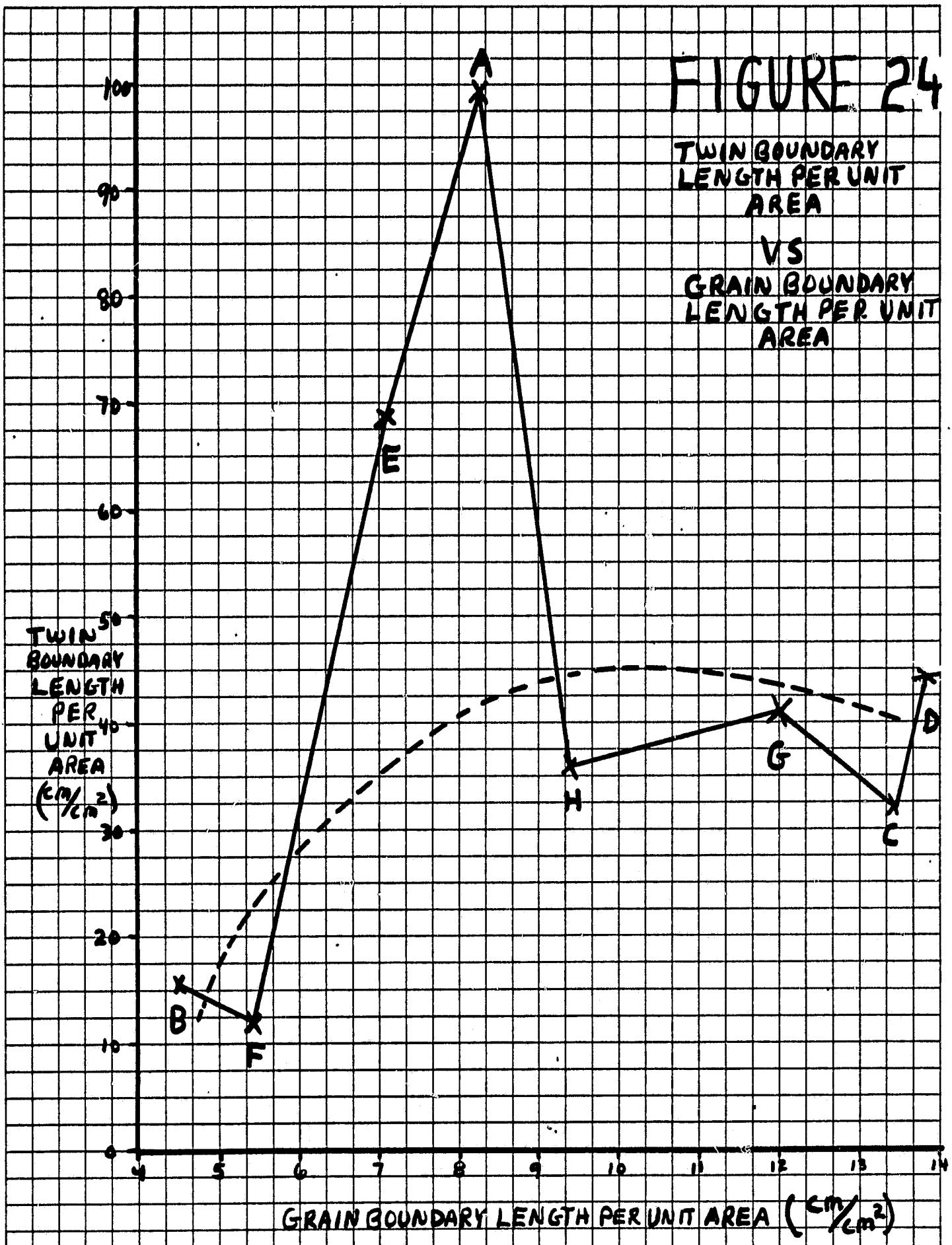

SECTION VII

APPENDIX

TABLES 1 THRU 24 LISTS ACTUAL DATA MEASURED

TABLE 1. Grain Boundary and Twin Boundary Density
SAMPLE SEMIX A-13 Sample in polished condition. Magnification 100X.
Field area = 0.0241 cm^2. Circumference of test circle = $\pi \cdot D$ = 0.55 cm.
A denotes No. of grain boundary intersections with circumference of test circle.
B denotes No. of twin boundary intersections with circumference of test circle.
X and Y denotes field location of the data measured.

FIELD			A	No. of twins	B
Y	No.	X			
12	1	33	7	33	24
12	2	35	7	28	37
12	3	37	2	137	201
12	4	39	4	12	23
12	5	41	2	113	119
12	6	43	2	9	14
12	7	45	3	15	10
12	8	47	6	26	31
12	9	49	0	0	0
12	10	51	0	0	0
14	11	50	2	0	0
14	12	47	2	12	12
14	13	44	0	2	4
14	14	41	2	124	196
14	15	38	2	19	33
14	16	35	7	40	47
16	17	34	0	0	0
16	18	36	3	27	28
16	19	38	3	12	15
16	20	40	5	50	47
16	21	42	2	1	2
16	22	44	2	8	8
16	23	46	4	9	8
16	24	48	0	0	0
16	25	50	2	0	0
18	26	49	3	20	6
18	27	46	5	14	9
18	28	43	2	4	6
18	29	40	4	6	11
18	30	37	6	8	4
20	31	37	4	39	19
20	32	39	2	10	8
20	33	41	3	3	3
20	34	43	2	2	2
20	35	45	0	1	2
20	36	47	2	0	0
10	37	50	8	32	3
10	38	47	5	24	25
10	39	44	2	9	9
10	40	41	4	14	12
10	41	38	2	112	198
10	42	35	6	21	24
8	43	34	5	33	42
8	44	36	2	29	41
8	45	38	4	144	257
8	46	40	2	12	22
8	47	42	2	20	9
8	48	44	2	0	0
8	49	46	0	15	30
8	50	48	4	63	29
8	51	50	2	7	11
6	52	49	4	29	33
6	53	46	0	13	23
6	54	43	2	5	9
6	55	40	4	20	24
6	56	37	4	38	62
4	57	37	6	117	148
4	58	39	2	100	160
4	59	41	3	42	37
4	60	43	2	3	4
4	61	45	0	0	0
4	62	47	0	2	4
Total for 62 fields:			179	1688	2145

L_A for grain boundary $= \frac{\pi}{2} \cdot P_L = \frac{\pi}{(2)(62)(0.55)} \frac{179}{} = 8.2 \frac{cm}{cm^2}$

L_A for twin boundary $= \frac{\pi \cdot 2145}{(2)(62)(0.55)} = 99 \ cm/cm^2$

$\bar{X}$ for grain boundary = 2.9
σ for grain boundary = 2.0

$\bar{X}$ for twin boundary = 34.6
σ for twin boundary = 56.5

$\frac{\pi}{2 \times 62 \times 0.55} = 0.046064484$, to be used for next seven tables for grain boundary & twin boundary density calculation

TABLE 2 Precipitate Particle Density

SAMPLE SEMIX A-13 Sample in polished condition. Magnification 400X

Field area = 0.00149 cm^2

A denotes No. of Large precipitates observed in field of view.

B denotes No. of Small precipitates observed in field of view.

X and Y denotes location of microscope stage for the data measured.

FIELD			A		B
Y	No.	X			
12	1	33	1		15
12	2	34	1		7
12	3	35	0		67
12	4	36	0		42
12	5	37	2		32
12	6	38	2		89
12	7	39	1		15
12	8	40	0		18
12	9	41	0		19
12	10	42	0		19
12	11	43	0		9
12	12	44	0		26
12	13	45	1		9
12	14	46	0		118
12	15	47	1		187
12	16	48	7		98
12	17	49	2		136
12	18	50	2		28
12	19	51	0		40
16	20	34	2		35
16	21	35	0		30
16	22	36	1		11
16	23	37	5		3
16	24	38	0		20
16	25	39	1		24
16	26	40	0		46
16	27	41	1		60
16	28	42	1		21
16	29	43	1		11
16	30	44	3		24
16	31	45	1		32
16	32	46	0		5
16	33	47	1		102
16	34	48	1		23
16	35	49	4		17
16	36	50	6		9
16	37	51	1		14
8	38	35	0		27
8	39	36	0		12
20	63	44	3		8
20	64	46	2		18

FIELD			A		B
Y	No.	X			
8	40	37	0		9
8	41	38	2		22
8	42	39	0		69
8	43	40	0		124
8	44	41	0		69
8	45	42	2		38
8	46	43	0		11
8	47	44	0		1
8	48	45	1		3
8	49	46	0		2
8	50	47	0		9
8	51	48	0		13
8	52	49	3		3
8	53	50	3		7
8	54	51	1		6
4	55	38	1		32
4	56	40	0		21
4	57	42	0		25
4	58	44	1		40
4	59	46	2		14
20	60	38	0		11
20	61	40	0		46
20	62	42	1		6
Total for 64 fields:			71		2107

Area of 64 fields = 0.09536 cm^2

No. of large ppt. = 71/0.09536

= 745/ cm^2

$\bar{X}$ for large ppt. = 1.1

σ for large ppt. = 1.5

No. of small ppt. = 2107/0.09536

= 22095 / cm^2

$\bar{X}$ for small ppt. = 33.0

σ for small ppt. = 36.5

TABLE 3 DISLOCATION DENSITY

SAMPLE SEMIX A-13. Sample in etched condition

Magnification 1000X, Area of field = 0.000238 cm^2

X and Y denote the location of microscope stage (field of view)for the data measured.

FIELD			No. of Dislocation Pits
Y	No.	X	↓
12	1	34	45
12	2	35	46
12	3	37	6
12	4	39	5
12	5	41	1
12	6	43	6
12	7	45	3
12	8	47	5
12	9	49	8
12	10	50	4
14	11	49	2
14	12	47	6
14	13	44	4
14	14	41	104
14	15	38	118
14	16	35	26
16	17	35	14
16	18	36	5
16	19	38	1
16	20	40	22
16	21	42	4
16	22	44	3
16	23	46	3
16	24	48	2
16	25	49	19
18	26	47	5
18	27	46	5
18	28	43	0
18	29	40	9
18	30	37	5
19	32	39	16
19	33	41	6
19	34	43	15
19	35	45	3
19	36	47	8
10	37	50	3
10	38	47	3
10	39	44	0

FIELD			No. of Dislocation Pits
Y	No.	X	↓
10	40	41	1
10	41	38	75
10	42	35	2
8	44	36	4
8	45	38	5
8	46	40	8
8	47	42	1
8	48	44	5
8	49	46	2
8	50	48	1
8	51	49	0
6	52	49	1
6	53	46	4
6	54	43	6
6	55	40	7
6	56	37	6
5	58	39	2
5	59	41	4
5	60	43	3
5	61	45	4
Total for fields:		58	681

Dislocation density

$= 681/(58)(0.000238)$ pits $/cm^2$

$= 4.9 \times 10^4$ pits $/cm^2$

$\overline{X} = 12$

$\sigma = 23$

TABLE 4 Grain Boundary and Twin Boundary Density

SAMPLE SEMIX B-2, Sample in polished condition. Magnification 100X. Field area = 0.0241 cm^2. Circumference of test circle = $\pi \cdot D$ = 0.55 cm.

A denotes No. of grain boundary intersections with circumference of test circle.

B denotes No. of twin boundary intersections with circumference of test circle.

X and Y denotes field location of the data measured.

FIELD			A	No. of twins	B
Y	No.	X			
12	1	33	7		15
12	2	35	3		25
12	3	37	0		0
12	4	39	0		4
12	5	41	0		2
12	6	43	0		0
12	7	45	0		0
12	8	47	0		0
12	9	49	0		0
12	10	51	4		29
14	11	50	0		0
14	12	47	0		0
14	13	44	0		0
14	14	41	0		4
14	15	38	0		0
14	16	35	6		1
16	17	34	8		3
16	18	36	3		6
16	19	38	2		4
16	20	40	0		0
16	21	42	0		0
16	22	44	0		4
16	23	46	0		0
16	24	48	0		0
16	25	50	0		0
18	26	49	0		0
18	27	46	0		7
18	28	43	0		0
18	29	40	2		4
18	30	37	2		3
20	31	37	2		8
20	32	39	2		30
20	33	41	2		8
20	34	43	1		6
20	35	45	0		0
20	36	47	0		0
10	37	50	6		50
10	38	47	0		2
10	39	44	0		0
10	40	41	2		0
10	41	38	2		4
10	42	35	4		17
8	43	34	7		16
8	44	36	6		25
8	45	38	4		7
8	46	40	2		0
8	47	42	0		0
8	48	44	0		0
8	49	46	0		7
8	50	48	0		17
8	51	50	3		7
6	52	49	0		3
6	53	46	0		0
6	54	43	0		0
6	55	40	5		3
6	56	37	2		0
4	57	37	5		10
4	58	39	4		6
4	59	41	2		7
4	60	43	0		0
4	61	45	0		1
4	62	47	0		2
Total for 62 fields:			98		347

L_A for grain boundary $= \frac{\pi}{2} \times P_L = \frac{\pi \times 98}{2 \times 62 \times 0.55} = 4.51 \frac{cm}{cm^2}$

L_A for twin boundary $= \frac{\pi \times 342}{2 \times 62 \times 0.55} = 15.75 \frac{cm}{cm^2}$

$\overline{X}$ for grain boundary = 1.6

σ for grain boundary = 2.2

$\overline{X}$ for twin boundary = 5.6

σ for twin boundary = 9.3

TABLE 5 Precipitate Particle Density

SAMPLE SEMIX B-2. Sample in polished condition. Magnification 400X.

Field area = 0.00149 cm^2

A denotes No. of Large precipitates observed in field of view.

B denotes No. of Small precipitates observed in field of view.

X and Y denotes location of microscope stage for the data measured.

FIELD			A		B
Y	No.	X			
12	1	33	2		14
12	2	35	0		24
12	3	37	0		18
12	4	39	1		18
12	5	41	0		25
12	6	43	0		22
12	7	45	1		11
12	8	47	0		71
12	9	49	0		31
12	10	51	0		27
14	11	50	0		34
14	12	47	3		86
14	13	44	2		23
14	14	41	1		32
14	15	38	0		44
14	16	35	0		38
16	17	34	1		13
16	18	36	0		14
16	19	38	0		35
16	20	40	2		13
16	21	42	0		23
16	22	44	0		17
16	23	46	0		38
16	24	48	0		15
16	25	50	1		36
18	26	49	3		13
18	27	46	3		48
18	28	43	2		23
18	29	40	0		9
18	30	37	2		27
20	31	37	4		34
20	32	39	0		28
20	33	41	0		20
20	34	43	1		39
20	35	45	0		14
20	36	47	1		13
10	37	50	1		27
10	38	47	1		14
10	39	44	0		17

FIELD			A		B
Y	No.	X			
10	40	41	0		9
10	41	38	1		22
10	42	35	0		31
8	43	34	0		19
8	44	36	1		17
8	45	38	0		22
8	46	40	1		16
8	47	42	0		33
8	48	44	1		16
8	49	46	0		66
8	50	48	0		59
8	51	50	0		59
6	52	49	0		27
6	53	46	0		22
6	54	43	0		18
6	55	40	1		14
6	56	37	1		15
4	57	37	0		25
4	58	39	2		95
4	59	41	0		36
4	60	43	1		64
4	61	45	0		40
4	62	47	0		29
Total for 62 fields:			41		1802

Area of 62 fields = 0.09238 cm^2

No. of large ppt. = 41 /0.09238
= 444/ cm^2

$\bar{X}$ for large ppt. = 0.66

σ for large ppt. = 0.95

No. of small ppt. = 1802 /0.09238
=19506 / cm^2

$\bar{X}$ for small ppt. = 29.1

σ for small ppt. = 18.1

TABLE 6 DISLOCATION DENSITY

SAMPLE SEMIX B-2. Sample in etched condition

Magnification 1000X, Area of field = 0.000238 cm^2

X and Y denote the location of microscope stage (field of view)for the data measured.

FIELD			No. of Dislocation Pits
Y	No.	X	
12	1	34	10
12	2	35	7
12	3	37	30
12	4	39	10
12	5	41	7
12	6	43	8
12	7	45	22
12	8	47	8
12	9	49	69
12	10	50	61
14	11	49	47
14	12	47	48
14	13	44	10
14	14	41	6
14	15	38	13
14	16	35	1
16	17	35	1
16	18	36	0
16	19	38	28
16	20	40	2
16	21	42	16
16	22	44	7
16	23	46	16
16	24	48	6
16	25	49	13
18	26	47	17
18	27	46	24
18	28	43	2
18	29	40	5
18	30	37	0
19	31	37	
19	32	39	
19	33	41	9
19	34	43	52
19	35	45	20
19	36	47	
10	37	50	294
10	38	47	5
10	39	44	4
10	40	41	21
10	41	38	1
10	42	35	6
8	43	35	
8	44	36	3
8	45	38	34
8	46	40	183
8	47	42	13
8	48	44	25
8	49	46	18
8	50	48	14
8	51	49	
6	52	49	2
6	53	46	5
6	54	43	1
6	55	40	3
6	56	37	5
5	57	38	
5	58	39	7
5	59	41	6
5	60	43	14
5	61	45	12
5	62	47	15
Total for 56 fields:			1266

Dislocation density

= 1266 /(56)(0.000238) pits /cm^2

= 0.95 x 10^5 pits /cm^2

$\overline{X}$ = 23

σ = 45

TABLE 7 Grain Boundary and Twin Boundary Density

SAMPLE SEMIX C-12. Sample in polished condition. Magnification 100X.

Field area = 0.0241 cm^2. Circumference of test circle = $\pi \cdot D$ = 0.55 cm.

A denotes No. of grain boundary intersections with circumference of test circle.

B denotes No. of twin boundary intersections with circumference of test circle.

X and Y denotes field location of the data measured.

FIELD			A	No. of twins	B
Y	No.	X			
12	1	33	8	17	11
12	2	35	10	20	24
12	3	37	3	14	19
12	4	39	2	24	30
12	5	41	4	25	32
12	6	43	4	2	2
12	7	45	8	1	1
12	8	47	0	0	0
12	9	49	4	5	5
12	10	51	6	9	8
14	11	50	10	29	11
14	12	47	7	11	4
14	13	44	5	6	5
14	14	41	2	9	10
14	15	38	5	11	18
14	16	35	9	22	16
16	17	34	3	2	2
16	18	36	3	7	6
16	19	38	7	6	6
16	20	40	8	8	6
16	21	42	4	3	6
16	22	44	2	2	4
16	23	46	3	1	1
16	24	48	7	5	4
16	25	50	4	28	25
18	26	49	8	20	15
18	27	46	9	3	2
18	28	43	4	1	1
18	29	40	3	2	1
18	30	37	3	11	10
20	31	37	7	3	3
20	32	39	3	6	6
20	33	41	5	0	0
20	34	43	5	2	4
20	35	45	7	0	0
20	36	47	5	1	1
10	37	50	2	5	4
10	38	47	4	6	5
10	39	44	7	5	5
10	40	41	4	45	57
10	41	38	10	9	8
10	42	35	2	19	22
8	43	34	7	17	15
8	44	36	0	13	26
8	45	38	6	19	22
8	46	40	8	15	12
8	47	42	0	8	9
8	48	44	4	28	15
8	49	46	4	6	3
8	50	48	6	11	11
8	51	50	2	3	6
6	52	49	5	9	12
6	53	46	7	12	7
6	54	43	0	22	25
6	55	40	3	38	43
6	56	37	0	8	10
4	57	37	0	3	6
4	58	39	3	11	14
4	59	41	8	59	29
4	60	43	3	22	22
4	61	45	4	11	4
4	62	47	4	3	2
Total for 62 fields:			290	723	693

L_A for grain boundary $= \frac{\pi}{2} \cdot P_L = \frac{\pi}{2} \frac{290}{x62 \times 0.55} = 13.36 \frac{cm}{cm^2}$

L_A for twin boundary $= \frac{\pi \times 693}{2 \times 62 \times 0.55} = 31.92 \frac{cm}{cm^2}$

$\overline{X}$ for grain boundary = 4.7

σ for grain boundary = 2.7

$\overline{X}$ for twin boundary = 11.2

σ for twin boundary = 11.1

TABLE 8 Precipitate Particle Density

SAMPLE SEMIX C-12 Sample in polished condition. Magnification 400X.

Field area = 0.00149 cm^2

A denotes No. of Large precipitates observed in field of view.

B denotes No. of Small precipitates observed in field of view.

X and Y denotes location of microscope stage for the data measured.

FIELD			A		B
Y	No.	X			
12	1	33	4		0
12	2	35	11		0
12	3	37	8		0
12	4	39	7		0
12	5	41	7		0
12	6	43	12		0
12	7	45	15		0
12	8	47	4		0
12	9	49	10		0
12	10	51	14		0
14	11	50	8		0
14	12	47	10		0
14	13	44	15		0
14	14	41	5		0
14	15	38	14		0
14	16	35	12		0
16	17	34	19		0
16	18	36	4		0
16	19	38	6		0
16	20	40	0		0
16	21	42	2		0
16	22	44	0		0
16	23	46	17		0
16	24	48	27		0
16	25	50	10		0
18	26	49	18		0
18	27	46	13		0
18	28	43	7		0
18	29	40	29		0
18	30	37	8		0
20	31	37	4		0
20	32	39	8		1
20	33	41	3		0
20	34	43	3		0
20	35	45	2		0
20	36	47	0		0
10	37	50	3		0
10	38	47	9		0
10	39	44	2		0

FIELD			A		B
Y	No.	X			
10	40	41	1		0
10	41	38	0		0
10	42	35	3		0
8	43	34	6		0
8	44	36	7		0
8	45	38	0		0
8	46	40	3		0
8	47	42	0		0
8	48	44	5		0
8	49	46	6		0
8	50	48	10		0
8	51	50	7		0
6	52	49	20		0
6	53	46	17		1
6	54	43	5		0
6	55	40	12		2
6	56	37	8		0
4	57	37	18		0
4	58	39	16		0
4	59	41	26		0
4	60	43	5		0
4	61	45	22		2
4	62	47	35		0
Total for 62 fields:			572		6

Area of 62 fields = 0.09238 cm^2

No. of large ppt. = 6 /0.09238

= 65 / cm^2

$\bar{X}$ for large ppt. = 0.1

σ for large ppt. = 0.4

No. of small ppt. = 572 /0.09238

= 6192 / cm^2

$\bar{X}$ for small ppt. = 9.2

σ for small ppt. = 7.7

TABLE 9 DISLOCATION DENSITY

SAMPLE SEMIX C-12. Sample in etched condition

Magnification 1000X, Area of field = 0.000238 cm^2

X and Y denote the location of microscope stage (field of view)for the data measured.

FIELD			No. of Dislocation Pits ↓
Y	No.	X	
12	1	34	26
12	2	35	187
12	3	37	114
12	4	39	58
12	5	41	17
12	6	43	33
12	7	45	29
12	8	47	101
12	9	49	15
12	10	50	11
14	11	49	55
14	12	47	162
14	13	44	11
14	14	41	20
14	15	38	185
14	16	35	253
16	17	35	136
16	18	36	82
16	19	38	205
16	20	40	37
16	21	42	52
16	22	44	52
16	23	46	47
16	24	48	44
16	25	49	177
18	26	47	265
18	27	46	34
18	28	43	90
18	29	40	43
18	30	37	31
19	31	37	
19	32	39	
19	33	41	10
19	34	43	8
19	35	45	
19	36	47	
10	37	50	165
10	38	47	82
10	39	44	48

FIELD			No. of Dislocation Pits ↓
Y	No.	X	
10	40	41	104
10	41	38	149
10	42	35	132
8	43	35	89
8	44	36	170
8	45	38	97
8	46	40	59
8	47	42	75
8	48	44	99
8	49	46	143
8	50	48	35
8	51	49	83
6	52	49	
6	53	46	81
6	54	43	121
6	55	40	108
6	56	37	133
5	57	38	66
5	58	39	96
5	59	41	152
5	60	43	73
5	61	45	45
5	62	47	
Total for 56 fields:			4989

Dislocation density

$= 4989/(56)(0.000238 \text{ pits}/cm^2$

$= 3.7 \times 10^5 \text{ pits}/cm^2$

$\bar{X} = 89$

$\sigma = 62$

TABLE 10 Grain Boundary and Twin Boundary Density
SAMPLE SEMIX D-8.2 Sample in polished condition. Magnification 100X.
Field area = 0.0241 cm^2. Circumference of test circle = $\pi \cdot D$ = 0.55 cm.
A denotes No. of grain boundary intersections with circumference of test circle.
B denotes No. of twin boundary intersections with circumference of test circle.
X and Y denotes field location of the data measured.

FIELD			A	No. of twins	B
Y	No.	X			
12	1	33	10	89	23
12	2	35	3	3	6
12	3	37	4	9	8
12	4	39	4	2	1
12	5	41	4	8	8
12	6	43	2	14	22
12	7	45	2	3	6
12	8	47	0	0	0
12	9	49	4	22	24
12	10	51	3	0	0
14	11	50	4	6	6
14	12	47	2	1	1
14	13	44	4	5	6
14	14	41	11	5	3
14	15	38	4	13	13
14	16	35	6	9	11
16	17	34	6	24	19
16	18	36	2	11	12
16	19	38	3	7	7
16	20	40	7	23	29
16	21	42	5	48	21
16	22	44	2	0	0
16	23	46	2	0	0
16	24	48	2	1	1
16	25	50	5	16	15
18	26	49	4	1	1
18	27	46	0	0	0
18	28	43	4	0	0
18	29	40	8	57	56
18	30	37	7	16	16
20	31	37	9	31	28
20	32	39	10	26	17
20	33	41	6	68	51
20	34	43	2	72	57
20	35	45	2	4	11
20	36	47	0	0	0
10	37	50	2	6	9
10	38	47	2	3	3
10	39	44	4	24	10
10	40	41	6	22	10
10	41	38	6	0	0
10	42	35	5	24	17
8	43	34	8	58	37
8	44	36	11	38	37
8	45	38	17	35	8
8	46	40	12	1	2
8	47	42	6	17	15
8	48	44	10	92	75
8	49	46	2	47	61
8	50	48	3	26	36
8	51	50	2	10	10
6	52	49	5	2	2
6	53	46	8	52	40
6	54	43	6	0	0
6	55	40	7	17	14
6	56	37	4	127	35
4	57	37	5	29	25
4	58	39	4	13	16
4	59	41	3	4	5
4	60	43	0	0	0
4	61	45	4	33	11
4	62	47	4	12	10
Total for 62 fields:			299	1295	967

L_A for grain boundary $= \frac{\pi}{2} \cdot P_L = \frac{\pi}{2 \times 62 \times 0.55} \frac{299}{} = 13.77 \frac{cm}{cm^2}$

L_A for twin boundary $= \frac{\pi \times 967}{2 \times 62 \times 0.55} = 44.54 \frac{cm}{cm^2}$

$\overline{X}$ for grain boundary = 4.8
σ for grain boundary = 3.2

$\overline{X}$ for twin boundary = 15.6
σ for twin boundary = 17.1

TABLE 11 Precipitate Particle Density

SAMPLE SEMIX D-8. Sample in polished condition. Magnification 400X.

Field area = 0.00149 cm^2

A denotes No. of Large precipitates observed in field of view.

B denotes No. of Small precipitates observed in field of view.

X and Y denotes location of microscope stage for the data measured.

FIELD			A		B
Y	No.	X			
12	1	33	0		9
12	2	35	0		10
12	3	37	0		2
12	4	39	0		5
12	5	41	1		0
12	6	43	0		7
12	7	45	0		17
12	8	47	0		3
12	9	49	0		4
12	10	51	2		6
14	11	50	0		2
14	12	47	0		3
14	13	44	0		1
14	14	41	1		2
14	15	38	0		0
14	16	35	0		9
16	17	34	1		1
16	18	36	0		0
16	19	38	0		4
16	20	40	1		3
16	21	42	0		7
16	22	44	1		0
16	23	46	0		5
16	24	48	0		7
16	25	50	0		8
18	26	49	1		2
18	27	46	0		1
18	28	43	1		3
18	29	40	0		0
18	30	37	0		3
20	31	37	0		6
20	32	39	0		3
20	33	41	0		3
20	34	43	0		2
20	35	45	1		2
20	36	47	1		7
10	37	50	0		1
10	38	47	0		0
10	39	44	0		1
10	40	41	0		0
10	41	38	1		0
10	42	35	0		11
8	43	34	0		4
8	44	36	0		1
8	45	38	0		0
8	46	40	1		1
8	47	42	0		0
8	48	44	1		0
8	49	46	0		2
8	50	48	0		2
8	51	50	0		1
6	52	49	0		8
6	53	46	0		2
6	54	43	0		0
6	55	40	0		0
6	56	37	0		7
4	57	37	0		16
4	58	39	0		6
4	59	41	0		2
4	60	43	0		4
4	61	45	0		16
4	62	47	0		3
Total for 62 fields:			14		235

Area of 62 fields = 0.09238 cm^2

No. of large ppt. = 14/0.09238

= 152/ cm^2

$\bar{X}$ for large ppt. = 0.23

σ for large ppt. = 0.46

No. of small ppt. = 235/0.09238

= 2544 / cm^2

$\bar{X}$ for small ppt. = 3.8

σ for small ppt. = 4.0

TABLE 12 DISLOCATION DENSITY

SAMPLE SEMIX D-8. Sample in etched condition

Magnification 1000X, Area of field = 0.000238 cm^2

X and Y denote the location of microscope stage (field of view)for the data measured.

FIELD			No. of Dislocation Pits ↓
Y	No.	X	
12	1	34	7
12	2	35	5
12	3	37	0
12	4	39	9
12	5	41	64
12	6	43	7
12	7	45	2
12	8	47	8
12	9	49	3
12	10	50	
14	11	49	14
14	12	47	6
14	13	44	2
14	14	41	3
14	15	38	2
14	16	35	4
16	17	35	
16	18	36	29
16	19	38	5
16	20	40	10
16	21	42	2
16	22	44	9
16	23	46	5
16	24	48	7
16	25	49	6
18	26	47	7
18	27	46	8
18	28	43	142
18	29	40	49
18	30	37	5
19	31	37	6
19	32	39	196
19	33	41	20
19	34	43	6
19	35	45	7
19	36	47	
10	37	50	12
10	38	47	19
10	39	44	15
10	40	41	12
10	41	38	7
10	42	35	5
8	43	35	2
8	44	36	2
8	45	38	15
8	46	40	11
8	47	42	304
8	48	44	7
8	49	46	2
8	50	48	8
8	51	49	
6	52	49	5
6	53	46	34
6	54	43	3
6	55	40	48
6	56	37	2
5	57	38	
5	58	39	95
5	59	41	6
5	60	43	5
5	61	45	14
5	62	47	89
Total for 57 fields:			1377

Dislocation density

$= 1377/(57)(0.000238)$ pits $/cm^2$

$= 1.0 \times 10^5$ pits $/cm^2$

$\bar{X} = 24$

$\sigma = 51$

TABLE 13 Grain Boundary and Twin Boundary Density

SAMPLE SEMIX E-13. Sample in polished condition. Magnification 100X. Field area = 0.0241 cm^2. Circumference of test circle = $\pi \cdot D$ = 0.55 cm.

A denotes No. of grain boundary intersections with circumference of test circle.

B denotes No. of twin boundary intersections with circumference of test circle.

X and Y denotes field location of the data measured.

FIELD			A	No. of twins	B
Y	No.	X			
12	1	33	4	7	7
12	2	35	2	5	7
12	3	37	0	4	6
12	4	39	0	1	2
12	5	41	2	38	35
12	6	43	0	0	0
12	7	45	2	0	0
12	8	47	0	0	0
12	9	49	0	0	0
12	10	51	0	0	0
14	11	50	0	0	0
14	12	47	0	1	1
14	13	44	0	0	0
14	14	41	0	0	0
14	15	38	2	13	13
14	16	35	0	4	7
16	17	34	0	0	0
16	18	36	4	6	3
16	19	38	0	0	0
16	20	40	2	15	15
16	21	42	7	18	10
16	22	44	6	20	17
16	23	46	4	51	51
16	24	48	6	33	39
16	25	50	6	53	74
18	26	49	3	69	57
18	27	46	2	10	11
18	28	43	0	0	0
18	29	40	0	0	0
18	30	37	2	0	0
20	31	37	0	0	0
20	32	39	0	0	0
20	33	41	0	0	0
20	34	43	0	0	0
20	35	45	2	1	1
20	36	47	2	8	7
10	37	50	3	21	17
10	38	47	2	4	4
10	39	44	3	4	3
10	40	41	2	170	124
10	41	38	5	27	29
10	42	35	3	3	2
8	43	34	5	0	0
8	44	36	7	12	8
8	45	38	6	8	6
8	46	40	3	12	20
8	47	42	2	8	15
8	48	44	2	16	24
8	49	46	6	34	50
8	50	48	4	86	94
8	51	50	3	102	161
6	52	49	2	71	132
6	53	46	4	92	152
6	54	43	4	43	71
6	55	40	4	26	38
6	56	37	2	0	0
4	57	37	3	2	2
4	58	39	3	25	24
4	59	41	3	33	45
4	60	43	3	24	38
4	61	45	7	17	24
4	62	47	4	26	42
Total for 62 fields:			153	1223	1488

L_A for grain boundary $= \frac{\pi}{2} \cdot P_L = \frac{\pi}{2} \frac{153}{62 \times 0.55} = 7.05 \frac{cm}{cm^2}$

L_A for twin boundary $= \frac{\pi \times 1488}{2 \times 62 \times 0.55} = 68.54 \frac{cm}{cm^2}$

$\bar{X}$ for grain boundary = 2.5

σ for grain boundary = 2.1

$\bar{X}$ for twin boundary = 24

σ for twin boundary = 37.7

TABLE 14 Precipitate Particle Density

SAMPLE SEMIX E-13. Sample in polished condition. Magnification 400X.

Field area = 0.00149 cm^2

A denotes No. of Large precipitates observed in field of view.

B denotes No. of Small precipitates observed in field of view.

X and Y denotes location of microscope stage for the data measured.

FIELD			A		B
Y	No.	X			
12	1	33	1		22
12	2	35	0		13
12	3	37	0		7
12	4	39	0		18
12	5	41	2		15
12	6	43	2		12
12	7	45	2		15
12	8	47	1		4
12	9	49	1		19
12	10	51	0		30
14	11	50	0		48
14	12	47	2		12
14	13	44	0		4
14	14	41	0		12
14	15	38	1		12
14	16	35	1		16
16	17	34	0		8
16	18	36	0		5
16	19	38	1		13
16	20	40	0		8
16	21	42	1		9
16	22	44	1		7
16	23	46	0		19
16	24	48	1		10
16	25	50	0		15
18	26	49	1		11
18	27	46	1		6
18	28	43	0		17
18	29	40	1		11
18	30	37	0		21
20	31	37	0		9
20	32	39	0		10
20	33	41	0		59
20	34	43	1		19
20	35	45	1		9
20	36	47	1		4
10	37	50	0		27
10	38	47	1		21
10	39	44	2		3

FIELD			A		B
Y	No.	X			
10	40	41	1		5
10	41	38	0		10
10	42	35	0		4
8	43	34	0		48
8	44	36	0		13
8	45	38	0		4
8	46	40	0		8
8	47	42	0		20
8	48	44	1		5
8	49	46	2		7
8	50	48	2		6
8	51	50	1		23
6	52	49	1		7
6	53	46	1		6
6	54	43	0		19
6	55	40	1		16
6	56	37	0		8
4	57	37	0		5
4	58	39	0		5
4	59	41	0		7
4	60	43	0		10
4	61	45	0		7
4	62	47	1		17
Total for 62 fields:			37		840

Area of 62 fields = 0.09238 cm^2

No. of large ppt. = 37/0.09238

= 400 / cm^2

$\bar{X}$ for large ppt. = 0.6

σ for large ppt. = 0.7

No. of small ppt. = 840/0.09238

= 9090 / cm^2

$\bar{X}$ for small ppt. = 13.5

σ for small ppt. = 10.6

TABLE 15 DISLOCATION DENSITY

SAMPLE SEMIX E-13. Sample in etched condition

Magnification 1000X, Area of field = 0.000238 cm^2

X and Y denote the location of microscope stage (field of view)for the data measured.

FIELD			No. of Dislocation Pits
Y	No.	X	↓
12	1	34	175
12	2	35	141
12	3	37	245
12	4	39	56
12	5	41	39
12	6	43	19
12	7	45	4
12	8	47	140
12	9	49	111
12	10	50	285
14	11	49	74
14	12	47	106
14	13	44	6
14	14	41	19
14	15	38	9
14	16	35	14
16	17	35	2
16	18	36	4
16	19	38	24
16	20	40	2
16	21	42	32
16	22	44	6
16	23	46	38
16	24	48	21
16	25	49	
18	26	47	9
18	27	46	35
18	28	43	14
18	29	40	2
18	30	37	11
19	31	37	
19	32	39	34
19	33	41	11
19	34	43	52
19	35	45	2
19	36	47	
10	37	50	360
10	38	47	370
10	39	44	250
10	40	41	242
10	41	38	93
10	42	35	68
8	43	35	295
8	44	36	97
8	45	38	58
8	46	40	170
8	47	42	235
8	48	44	187
8	49	46	188
8	50	48	203
8	51	49	102
6	52	49	
6	53	46	70
6	54	43	39
6	55	40	78
6	56	37	62
5	57	38	
5	58	39	22
5	59	41	22
5	60	43	35
5	61	45	38
5	62	47	
Total for 56 fields:			4996

Dislocation density

$= 4996/(56)(0.000238)$ pits $/cm^2$

$= 3.7 \times 10^5$ pits $/cm^2$

$\overline{X} = 89$

$\sigma = 96$

TABLE 16 Grain Boundary and Twin Boundary Density
SAMPLE SEMIX F-2, Sample in polished condition. Magnification 100X.
Field area = 0.0241 cm^2. Circumference of test circle = $\pi \cdot D$ = 0.55 cm.
A denotes No. of grain boundary intersections with circumference of test circle.
B denotes No. of twin boundary intersections with circumference of test circle.
X and Y denotes field location of the data measured.

FIELD			A	No. of twins	B
Y	No.	X			
12	1	33	0	6	9
12	2	35	0	4	7
12	3	37	0	0	0
12	4	39	0	0	0
12	5	41	2	0	0
12	6	43	0	0	0
12	7	45	0	0	0
12	8	47	0	0	0
12	9	49	0	2	4
12	10	51	3	3	2
14	11	50	2	19	28
14	12	47	0	0	0
14	13	44	0	0	0
14	14	41	5	0	0
14	15	38	5	0	0
14	16	35	3	28	12
16	17	34	2	30	27
16	18	36	2	26	24
16	19	38	2	3	3
16	20	40	4	10	12
16	21	42	2	5	5
16	22	44	0	0	0
16	23	46	3	1	2
16	24	48	6	12	10
16	25	50	5	11	16
18	26	49	5	3	3
18	27	46	3	2	3
18	28	43	5	5	4
18	29	40	2	6	9
18	30	37	3	46	22
20	31	37	3	3	5
20	32	39	6	6	2
20	33	41	9	10	8
20	34	43	7	5	4
20	35	45	7	2	8
20	36	47	11	3	1
10	37	50	0	0	0
10	38	47	0	2	4
10	39	44	0	0	0
10	40	41	0	0	0
10	41	38	0	0	0
10	42	35	0	0	0
8	43	34	0	0	0
8	44	36	0	0	0
8	45	38	0	0	0
8	46	40	0	0	0
8	47	42	0	0	0
8	48	44	0	0	0
8	49	46	0	0	0
8	50	48	0	2	4
8	51	50	0	0	0
6	52	49	0	1	2
6	53	46	0	0	0
6	54	43	0	0	0
6	55	40	2	6	6
6	56	37	0	0	0
4	57	37	0	0	0
4	58	39	4	5	5
4	59	41	5	19	13
4	60	43	0	0	0
4	61	45	0	0	0
4	62	47	0	0	0
Total for 62 fields:			118	287	264

L_A for grain boundary $= \frac{\pi}{2} \cdot P_L = \frac{\pi \times 118}{2 \times 62 \times 0.55} = 5.44 \frac{cm}{cm^2}$

L_A for twin boundary $= \frac{\pi \times 264}{2 \times 62 \times 0.55} = 12.16 \frac{cm}{cm^2}$

$\overline{X}$ for grain boundary = 1.9
σ for grain boundary = 2.6

$\overline{X}$ for twin boundary = 4.3
σ for twin boundary = 6.8

TABLE 17 Precipitate Particle Density

SAMPLE SEMIX F-2. Sample in polished condition. Magnification 400X.

Field area = 0.00149 cm^2

A denotes No. of Large precipitates observed in field of view.

B denotes No. of Small precipitates observed in field of view.

X and Y denotes location of microscope stage for the data measured.

FIELD			B		A
Y	No.	X			
12	1	33	11		1
12	2	35	4		0
12	3	37	35		3
12	4	39	43		2
12	5	41	2		0
12	6	43	26		13
12	7	45	3		0
12	8	47	26		3
12	9	49	6		1
12	10	51	34		0
14	11	50	35		2
14	12	47	3		0
14	13	44	3		1
14	14	41	6		1
14	15	38	8		0
14	16	35	0		0
16	17	34	6		0
16	18	36	1		3
16	19	38	5		0
16	20	40	1		1
16	21	42	2		0
16	22	44	4		1
16	23	46	5		0
16	24	48	0		0
16	25	50	1		2
18	26	49	0		1
18	27	46	0		0
18	28	43	1		0
18	29	40	1		2
18	30	37	1		0
20	31	37	3		0
20	32	39	2		2
20	33	41	1		0
20	34	43	0		1
20	35	45	0		0
20	36	47	4		0
10	37	50	7		8
10	38	47	1		0
10	39	44	16		0

FIELD			B		A
Y	No.	X			
10	40	41	42		0
10	41	38	7		0
10	42	35	15		0
8	43	34	3		5
8	44	36	7		2
8	45	38	7		3
8	46	40	4		2
8	47	42	2		0
8	48	44	0		0
8	49	46	5		0
8	50	48	1		0
8	51	50	5		1
6	52	49	0		0
6	53	46	4		1
6	54	43	2		0
6	55	40	6		2
6	56	37	3		1
4	57	37	6		2
4	58	39	2		0
4	59	41	3		0
4	60	43	2		1
4	61	45	6		0
4	62	47	0		0
Total for 62 fields:			447		68.

Area of 62 fields = 0.09238 cm^2

No. of large ppt. = 68 /0.09238

= 736/ cm^2

$\bar{X}$ for large ppt. = 1.1

σ for large ppt. = 2.1

No. of small ppt. = 447/0.09238

= 4840 / cm^2

$\bar{X}$ for small ppt. = 7.2

σ for small ppt. = 10.5

TABLE 18 DISLOCATION DENSITY

SAMPLE SEMIX F-2. Sample in etched condition

Magnification 1000X, Area of field = 0.000238 cm^2

X and Y denote the location of microscope stage (field of view)for the data measured.

FIELD			No. of Dislocation Pits
Y	No.	X	↓
12	1	34	7
12	2	35	0
12	3	37	15
12	4	39	14
12	5	41	16
12	6	43	7
12	7	45	4
12	8	47	7
12	9	49	2
12	10	50	4
14	11	49	6
14	12	47	2
14	13	44	4
14	14	41	5
14	15	38	5
14	16	35	12
16	17	35	8
16	18	36	3
16	19	38	3
16	20	40	13
16	21	42	7
16	22	44	5
16	23	46	110
16	24	48	1
16	25	49	3
18	26	47	9
18	27	46	188
18	28	43	9
18	29	40	13
18	30	37	47
19	31	37	
19	32	39	36
19	33	41	850
19	34	43	44
19	35	45	
19	36	47	
10	37	50	23
10	38	47	36
10	39	44	31
10	40	41	41
10	41	38	47
10	42	35	34
8	43	35	22
8	44	36	18
8	45	38	22
8	46	40	37
8	47	42	127
8	48	44	58
8	49	46	25
8	50	48	38
8	51	49	22
6	52	49	16
6	53	46	29
6	54	43	68
6	55	40	16
6	56	37	20
5	57	38	21
5	58	39	19
5	59	41	45
5	60	43	14
5	61	45	26
5	62	47	20
Total for fields:		59	2334

Dislocation density

$= 2334/(59)(0.000238 \text{ pits/cm}^2$

$= 1.7 \times 10^5 \text{ pits / cm}^2$

$\overline{X} = 40$

$\sigma = 111$

TABLE 19 Grain Boundary and Twin Boundary Density

SAMPLE SEMIX G-12. Sample in polished condition. Magnification 100X.

Field area = 0.0241 cm^2. Circumference of test circle = $\pi \cdot D$ = 0.55 cm.

A denotes No. of grain boundary intersections with circumference of test circle.

B denotes No. of twin boundary intersections with circumference of test circle.

X and Y denotes field location of the data measured.

FIELD			A	No. of twins	B
Y	No.	X			
12	1	33	2	6	9
12	2	35	5	2	4
12	3	37	2	3	3
12	4	39	5	13	16
12	5	41	2	4	3
12	6	43	8	30	38
12	7	45	8	74	100
12	8	47	4	52	38
12	9	49	4	44	9
12	10	51	6	79	42
14	11	50	2	25	16
14	12	47	3	7	7
14	13	44	5	0	0
14	14	41	10	5	2
14	15	38	2	4	2
14	16	35	0	0	0
16	17	34	2	0	0
16	18	36	5	6	3
16	19	38	4	10	3
16	20	40	8	10	5
16	21	42	10	8	3
16	22	44	4	1	1
16	23	46	6	69	15
16	24	48	3	12	2
16	25	50	4	16	16
18	26	49	4	30	8
18	27	46	4	19	15
18	28	43	0	0	0
18	29	40	5	15	6
18	30	37	7	20	5
20	31	37	9	11	13
20	32	39	8	27	22
20	33	41	3	12	10
20	34	43	5	16	8
20	35	45	0	2	3
20	36	47	2	6	11
10	37	50	0	18	28
10	38	47	9	22	11
10	39	44	4	32	24
10	40	41	6	39	11
10	41	38	3	24	24
10	42	35	3	6	2
8	43	34	3	6	6
8	44	36	2	22	22
8	45	38	3	16	19
8	46	40	8	26	17
8	47	42	3	14	18
8	48	44	6	19	26
8	49	46	3	45	34
8	50	48	2	15	26
8	51	50	0	5	10
6	52	49	0	7	5
6	53	46	2	19	24
6	54	43	8	38	40
6	55	40	7	24	18
6	56	37	2	0	0
4	57	37	8	13	6
4	58	39	2	3	4
4	59	41	6	16	9
4	60	43	4	38	20
4	61	45	5	33	22
4	62	47	2	19	20
Total for 62 fields:			262	1157	884

L_A for grain boundary $= \frac{\pi}{2} \cdot P_L = \frac{\pi \times 262}{2 \times 62 \times 0.55} = 12.07 \frac{cm}{cm^2}$

L_A for twin boundary $= \frac{\pi \times 884}{2 \times 62 \times 0.55} = 40.72 \frac{cm}{cm^2}$

$\bar{X}$ for grain boundary = 4.2

σ for grain boundary = 2.6

$\bar{X}$ for twin boundary = 14.3

σ for twin boundary = 15.5

TABLE 20 Precipitate Particle Density

SAMPLE SEMIX G-12. Sample in polished condition. Magnification 400X.

Field area = 0.00149 cm^2

A denotes No. of Large precipitates observed in field of view.

B denotes No. of Small precipitates observed in field of view.

X and Y denotes location of microscope stage for the data measured.

FIELD			A		B
Y	No.	X			
12	1	33	0		16
12	2	35	0		18
12	3	37	1		3
12	4	39	0		9
12	5	41	1		15
12	6	43	0		8
12	7	45	0		1
12	8	47	0		2
12	9	49	0		7
12	10	51	0		11
14	11	50	1		2
14	12	47	0		27
14	13	44	0		8
14	14	41	0		26
14	15	38	1		5
14	16	35	0		8
16	17	34	0		36
16	18	36	0		40
16	19	38	0		12
16	20	40	1		21
16	21	42	0		9
16	22	44	1		2
16	23	46	1		12
16	24	48	0		1
16	25	50	0		3
18	26	49	0		14
18	27	46	0		1
18	28	43	1		9
18	29	40	0		20
18	30	37	0		12
20	31	37	0		7
20	32	39	0		5
20	33	41	0		6
20	34	43	0		7
20	35	45	0		0
20	36	47	0		13
10	37	50	0		10
10	38	47	1		4
10	39	44	0		9
10	40	41	0		6
10	41	38	0		9
10	42	35	1		9
8	43	34	0		3
8	44	36	0		6
8	45	38	0		2
8	46	40	0		3
8	47	42	0		2
8	48	44	1		17
8	49	46	0		2
8	50	48	1		16
8	51	50	0		14
6	52	49	0		3
6	53	46	0		10
6	54	43	1		11
6	55	40	0		2
6	56	37	0		15
4	57	37	0		13
4	58	39	0		4
4	59	41	0		11
4	60	43	0		1
4	61	45	0		11
4	62	47	0		4
Total for 62 fields:			13		593

Area of 62 fields = 0.09238 cm^2

No. of large ppt. = 13 / 0.09238
= 140 / cm^2

$\bar{X}$ for large ppt. = 0.21

σ for large ppt. = 0.41

No. of small ppt. = 593 / 0.09238
= 6420 / cm^2

$\bar{X}$ for small ppt. = 9.6

σ for small ppt. = 8.0

TABLE 21 DISLOCATION DENSITY
SAMPLE SEMIX G-12. Sample in etched condition
Magnification 1000X, Area of field = 0.000238 cm^2
X and Y denote the location of microscope stage (field of view)for the data measured.

FIELD			No. of Dislocation Pits ↓		
Y	No.	X			
12	1	34			
12	2	35		1	
12	3	37		2	
12	4	39		25	
12	5	41		0	
12	6	43		27	
12	7	45		0	
12	8	47		106	
12	9	49		187	
12	10	50		182	
14	11	49		125	
14	12	47		158	
14	13	44		163	
14	14	41		6	
14	15	38		92	
14	16	35		23	
16	17	35		21	
16	18	36		49	
16	19	38		89	
16	20	40		63	
16	21	42		10	
16	22	44		480	
16	23	46		310	
16	24	48		1000	
16	25	49		92	
18	26	47		23	
18	27	46		122	
18	28	43		15	
18	29	40		99	
18	30	37		74	
19	31	37			
19	32	39		108	
19	33	41		230	
19	34	43		450	
19	35	45		20	
19	36	47			
10	37	50		320	
10	38	47		275	
10	39	44		16	

FIELD			No. of Dislocation Pits ↓		
Y	No.	X			
10	40	41		33	
10	41	38		3	
10	42	35		3	
8	43	35			
8	44	36		0	
8	45	38		58	
8	46	40		127	
8	47	42		112	
8	48	44		78	
8	49	46		135	
8	50	48		15	
8	51	49			
6	52	49		72	
6	53	46		63	
6	54	43		15	
6	55	40		2	
6	56	37		10	
5	57	38			
5	58	39		85	
5	59	41		41	
5	60	43		70	
5	61	45		47	
5	62	47			
Total for 55 fields:				5932	

Dislocation density

$= 5932/(55)(0.000238)$ pits/cm^2

$= 4.5 \times 10^5$ pits/cm^2

$\bar{X} = 108$

$\sigma = 161$

TABLE 22 Grain Boundary and Twin Boundary Density

SAMPLE SEMIX H-8, Sample in polished condition. Magnification 100X. Field area = 0.0241 cm^2. Circumference of test circle = $\pi \cdot D$ = 0.55 cm.

A denotes No. of grain boundary intersections with circumference of test circle.

B denotes No. of twin boundary intersections with circumference of test circle.

X and Y denotes field location of the data measured.

FIELD			A	No. of twins	B
Y	No.	X			
12	1	33	8	44	19
12	2	35	3	4	5
12	3	37	4	9	8
12	4	39	2	4	3
12	5	41	5	6	6
12	6	43	2	10	11
12	7	45	2	1	2
12	8	47	2	3	1
12	9	49	5	13	12
12	10	51	4	3	3
14	11	50	2	10	12
14	12	47	2	2	2
14	13	44	2	4	4
14	14	41	2	4	2
14	15	38	5	15	10
14	16	35	3	12	15
16	17	34	6	19	18
16	18	36	2	12	17
16	19	38	2	2	2
16	20	40	6	17	24
16	21	42	6	39	34
16	22	44	0	1	2
16	23	46	3	2	2
16	24	48	3	2	2
16	25	50	6	1	2
18	26	49	2	0	0
18	27	46	0	0	0
18	28	43	3	6	8
18	29	40	3	4	45
18	30	37	3	17	19
20	31	37	5	12	9
20	32	39	4	22	18
20	33	41	5	48	44
20	34	43	2	54	68
20	35	45	2	13	13
20	36	47	0	0	0
10	37	50	2	4	5
10	38	47	0	0	0
10	39	44	3	13	6
10	40	41	3	15	9
10	41	38	2	2	2
10	42	35	5	15	13
8	43	34	7	20	24
8	44	36	6	17	17
8	45	38	3	4	4
8	46	40	3	1	1
8	47	42	2	17	5
8	48	44	5	54	39
8	49	46	0	14	28
8	50	48	4	9	11
8	51	50	0	7	9
6	52	49	4	11	10
6	53	46	4	21	34
6	54	43	4	37	18
6	55	40	7	8	11
6	56	37	4	113	28
4	57	37	6	50	31
4	58	39	2	7	13
4	59	41	3	3	3
4	60	43	0	0	0
4	61	45	6	35	6
4	62	47	4	4	4
Total for 62 fields:			205	931	779

L_A for grain boundary $= \frac{\pi}{2} \cdot P_L = \frac{\pi}{2} \frac{\times 205}{\times 62 \times 0.55} = 9.44 \frac{cm}{cm^2}$

L_A for twin boundary $= \frac{\pi \times 779}{2 \times 62 \times 0.55} = 35.88 \frac{cm}{cm^2}$

$\bar{X}$ for grain boundary = 3.3

σ for grain boundary = 1.9

$\bar{X}$ for twin boundary = 12.6

σ for twin boundary = 13.3

TABLE 23 Precipitate Particle Density

SAMPLE SEMIX H-8. Sample in polished condition. Magnification 400X.

Field area = 0.00149 cm^2

A denotes No. of Large precipitates observed in field of view.

B denotes No. of Small precipitates observed in field of view.

X and Y denotes location of microscope stage for the data measured.

FIELD			A		B
Y	No.	X			
12	1	33	2		48
12	2	35	2		3
12	3	37	0		13
12	4	39	0		7
12	5	41	0		9
12	6	43	1		14
12	7	45	0		8
12	8	47	0		5
12	9	49	1		6
12	10	51	1		9
14	11	50	0		17
14	12	47	0		9
14	13	44	1		14
14	14	41	0		19
14	15	38	0		11
14	16	35	0		28
16	17	34	1		14
16	18	36	0		5
16	19	38	0		3
16	20	40	0		4
16	21	42	0		11
16	22	44	0		1
16	23	46	0		5
16	24	48	0		7
16	25	50	0		8
18	26	49	0		3
18	27	46	0		10
18	28	43	3		18
18	29	40	0		3
18	30	37	0		14
20	31	37	0		37
20	32	39	2		52
20	33	41	0		11
20	34	43	0		22
20	35	45	1		9
20	36	47	0		15
10	37	50	0		7
10	38	47	0		3
10	39	44	1		15

FIELD			A		B
Y	No.	X			
10	40	41	0		10
10	41	38	4		10
10	42	35	0		38
8	43	34	0		41
8	44	36	0		19
8	45	38	0		25
8	46	40	0		12
8	47	42	1		7
8	48	44	0		11
8	49	46	0		23
8	50	48	1		14
8	51	50	0		18
6	52	49	0		19
6	53	46	0		34
6	54	43	0		8
6	55	40	0		4
6	56	37	0		9
4	57	37	1		13
4	58	39	0		9
4	59	41	0		6
4	60	43	0		16
4	61	45	0		17
4	62	47	0		15
Total for 62 fields:			23		875

Area of 62 fields = 0.09238 cm^2

No. of large ppt. = 23/0.09238
= 250/ cm^2

$\bar{X}$ for large ppt. = 0.4

σ for large ppt. = 0.8

No. of small ppt. = 875 /0.09238
= 9470 / cm^2

$\bar{X}$ for small ppt. = 14.1

σ for small ppt. = 10.9

TABLE 24 DISLOCATION DENSITY

SAMPLE SEMIX H-8. Sample in etched condition

Magnification 1000X, Area of field = 0.000238 cm^2

X and Y denote the location of microscope stage (field of view)for the data measured.

FIELD			No. of Dislocation Pits ↓	
Y	No.	X		
12	1	34	138	
12	2	35	103	
12	3	37	4	
12	4	39	71	
12	5	41	197	
12	6	43	215	
12	7	45	360	
12	8	47	222	
12	9	49	172	
12	10	50	155	
14	11	49	19	
14	12	47	3	
14	13	44	78	
14	14	41	6	
14	15	38	69	
14	16	35	125	
16	17	35		
16	18	36	320	
16	19	38	24	
16	20	40	248	
16	21	42	127	
16	22	44	17	
16	23	46	16	
16	24	48	2	
16	25	49	2	
18	26	47	310	
18	27	46	189	
18	28	43	271	
18	29	40	425	
18	30	37	219	
19	31	37	111	
19	32	39	303	
19	33	41	82	
19	34	43	300	
19	35	45	180	
19	36	47		
10	37	50	6	
10	38	47	307	
10	39	44	226	
10	40	41	164	
10	41	38	960	
10	42	35	72	
8	43	35		
8	44	36	49	
8	45	38	1050	
8	46	40	23	
8	47	42	725	
8	48	44	119	
8	49	46	325	
8	50	48	213	
8	51	49		
6	52	49	255	
6	53	46	32	
6	54	43	83	
6	55	40	1030	
6	56	37	3	
5	57	38		
5	58	39	21	
5	59	41	184	
5	60	43	228	
5	61	45	270	
5	62	47		
Total for 56 fields:			11428	

Dislocation density

$= 11428/(56)(0.000238)$ pits $/cm^2$

$= 8.6 \times 10^5$ pits $/cm^2$

$\bar{X} = 204$

$\sigma = 235$